Characterizing boreal forest wildfire with multi-temporal Landsat and LIDAR data

M.A. Wulder [a,*], J.C. White [a], F. Alvarez [b], T. Han [c], J. Rogan [d], B. Hawkes [a]

[a] Canadian Forest Service (Pacific Forestry Centre), Natural Resources Canada, Victoria, British Columbia, Canada V8Z 1M5
[b] Universidad de León, E.S.T. Ingenieros de Minas, Avd. Astorga s/n 24400, Ponferrada, Leon, Spain
[c] Integrated Land Management Bureau, Ministry of Agriculture and Lands, PO Box 9355 STN PROV GOVT, Victoria, British Columbia, Canada V8W 9M1
[d] Clark Graduate School of Geography, Clark University, Worcester, Massachusetts, USA 01610

ARTICLE INFO

ABSTRACT

Wildfire is an important disturbance agent in Canada's boreal forest. Optical remotely sensed imagery (e.g., Landsat TM/ETM+), is well suited for capturing horizontally distributed forest conditions, structure, and change, while Light Detection and Ranging (LIDAR) data are more appropriate for capturing vertically distributed elements of forest structure and change. The integration of optical remotely sensed imagery and LIDAR data provides improved opportunities to characterize post-fire conditions. The objective of this study is to compare changes in forest structure, as measured with a discrete return profiling LIDAR, to post-fire conditions, as measured with remotely sensed data. Our research is focused on a boreal forest fire that occurred in May 2002 in Alberta, Canada. The Normalized Burn Ratio (NBR), the differenced NBR (dNBR), and the relative dNBR (RdNBR) were calculated from two dates of Landsat data (August 2001 and September 2002). Forest structural attributes were derived from two spatially coincident discrete return LIDAR profiles acquired in September 1997 and 2002 respectively. Image segmentation was used to produce homogeneous spatial patches analogous to forest stands, with analysis conducted at this patch level.

In this study area, which was relatively homogenous and dominated by open forest, no statistically significant relationships were found between pre-fire forest structure and post-fire conditions ($r < 0.5$; $p > 0.05$). Post-fire forest structure and absolute and relative changes in forest structure were strongly correlated to post-fire conditions (r ranging from -0.507 to 0.712; $p < 0.0001$). Measures of vegetation fill (VF) (LIDAR capture of cross-sectional vegetation amount), post-fire and absolute change in crown closure (CC), and relative change in average canopy height, were most useful for characterizing post-fire conditions. Forest structural attributes generated from the post-fire LIDAR data were most strongly correlated to post-fire NBR, while dNBR and RdNBR had stronger correlations with absolute and relative changes in the forest structural attributes. Absolute and relative changes in VF and changes in CC had the strongest positive correlations with respect to dNBR and RdNBR, ranging from 0.514 to 0.715 ($p < 0.05$). Measures of average inter-tree distance and volume were not strongly correlated to post-fire NBR, dNBR, or RdNBR. No marked differences were found in the strength or significance of correlations between post-fire structure and the post-fire NBR, dNBR, RdNBR, indicating that for the conditions present in this study area all three burn severity indices captured post-fire conditions in a similar manner. Finally, the relationship between post-fire forest structure and post-fire condition was strongest for dense forests (>60% crown closure) compared to open (26–60%) and sparse forests (10–25%). Forest structure information provided by LIDAR is useful for characterizing post-fire conditions and burn induced structural change, and will complement other attributes such as vegetation type and moisture, topography, and long-term weather patterns, all of which will also influence variations in post-fire conditions.

1. Introduction

Wildfire events play an integral role in the ecological functioning of Canadian boreal forests (Bergeron et al., 2004; Parisien et al., 2006), impacting carbon emissions (Amiro et al., 2001; Stocks et al., 2002), plant reproduction (Johnstone & Kasischke, 2005; Johnstone & Chapin, 2006), forest succession (Harper et al., 2005; Lecomte et al., 2006), wildlife habitat quality (Dawson & Bartolotti, 2006), hydrology (Yoshikawa et al., 2003), and soil nutrient cycling (Zasada et al., 1992). Researchers have hypothesized the existence of a positive feedback loop between global warming and forest fires: global warming will extend the fire season in the boreal forest, increasing the likelihood of forest fires and further contributing to greenhouse gas emissions (Balshi et al., 2007; Gillett & Weaver, 2004; Kasischke et al., 1995; Soja et al., 2007; Stocks et al., 1998).

* Corresponding author. Canadian Forest Service, 506 West Burnside Road, Victoria, Canada BC V8Z 1M5. Tel.: +1 250 363 6090; fax: +1 250 363 0775.
E-mail address: mike.wulder@pfc.cfs.nrcan.gc.ca (M.A. Wulder).

Climate change scenarios produce an expectation of an increased likelihood of longer fire seasons with more frequent large, high intensity fire events (Flannigan et al., 2005a; Tymstra et al., 2007). It has been projected that increasing concentrations of CO_2 in the atmosphere could result in a 74–118% increase in the average annual area burned in Canada by the end of the 21st century (Flannigan et al., 2005b). Bond-Lamberty et al. (2007) assert that the impacts of climate change have yet to be realized in Canada's boreal forest region. Existing data indicates that the number of forest fires recorded in Canada have increased steadily over the past eight decades to approximately 8000 fires per annum in the 1990s, while the annual area burned has fluctuated substantially over this same time period (Stocks et al., 2003). Average fire suppression costs in Canada range from $300 to $500 million dollars annually (Flannigan et al., 2005b).

Due to broad ecological, social, and economic implications, there is much interest in characterizing forest fire fuels (Arroyo et al., 2008; Mutlu et al., 2008), forest fire behaviour (Pastor et al., 2003), and post-fire recovery (Shatford et al., 2007) for forest fire management. Post-fire conditions are often described in the context of fire intensity and fire or burn severity (Lentile et al., 2006a). Fires burn with varying intensities (i.e., energy released per unit length of flame front, per unit time), depending on fuel load, fuel moisture, wind speed, and topographic constraints (i.e., slope steepness and aspect) (Wright & Bailey, 1982). Fire or burn severity are measures used to characterize the degree to which the ecosystem is impacted by a fire (DeBano et al., 1998; Neary et al., 2005; Ryan, 2002) and incorporate both short- and long-term effects (Key, 2006; Key & Benson, 2006; Lentile et al., 2006a). To date, relatively few studies have used remotely sensed data, specifically LIDAR and optical imagery, to directly investigate the impact of wildfire on vertical forest structure (French et al., 2008).

The goal of this study was to relate variations in remotely sensed measures of post-fire effects to measures of pre- and post-fire vertical forest structure. The first objective was to evaluate whether LIDAR can be used to detect changes in vertical forest structural characteristics associated with wildfire. The second objective was to characterize the relationships between the vertical forest structural information afforded by discrete return profiling LIDAR data collected pre- and post-fire, with the horizontal information on pre- and post-fire vegetation location, type, and post-fire effects provided by Landsat Thematic Mapper (TM) and Enhanced Thematic Mapper Plus (ETM+) imagery acquired pre- and post-fire. This included examining post-fire forest structure, as well as absolute and relative changes in forest structure in the context of varying post-fire effects. The third objective was to determine the influence of pre-fire forest structure on post-fire effects.

2. Background

2.1. Post-fire effects

No common definition of fire or burn severity exists (Jain et al., 2004; Key & Benson, 2006) and both terms have been used interchangeably in the literature. Lentile et al. (2006a) suggest the use of the more generic term "post-fire effects" and distinguish between fire and burn severity as a function of time: fire severity is a measure of immediate post-fire effects such as direct vegetation consumption and mortality as a result of the fire, whereas burn severity is a measure of the longer term consequences of fire. There is often temporal overlap between these two assessments of severity (Lentile et al., 2006a).

For a given area, variation in vertical and horizontal forest structure and composition, and the attendant variation in fire intensity, result in variations in post-fire effects. Post-fire effects can range from partial consumption of vegetation cover with little soil exposure and, or light char/ash deposition, to complete consumption of vegetation cover with high soil exposure and heavy char/ash deposition (Rogan & Franklin, 2001; White et al., 1996). Severity can be a qualitative or quantitative assessment of the ecological effects of a fire that integrates the various phenomenological characteristics of a fire-altered landscape (i.e., the physical, biological, and chemical manifestations of combustion on vegetation) (Pyne et al., 1996). Knowledge of severity provides a vital source of information to understand the impact of fire on ecological functions and as a means to characterize the intensity of past, current, and future fire events (Epting et al., 2005; van Wagtendonk et al., 2004).
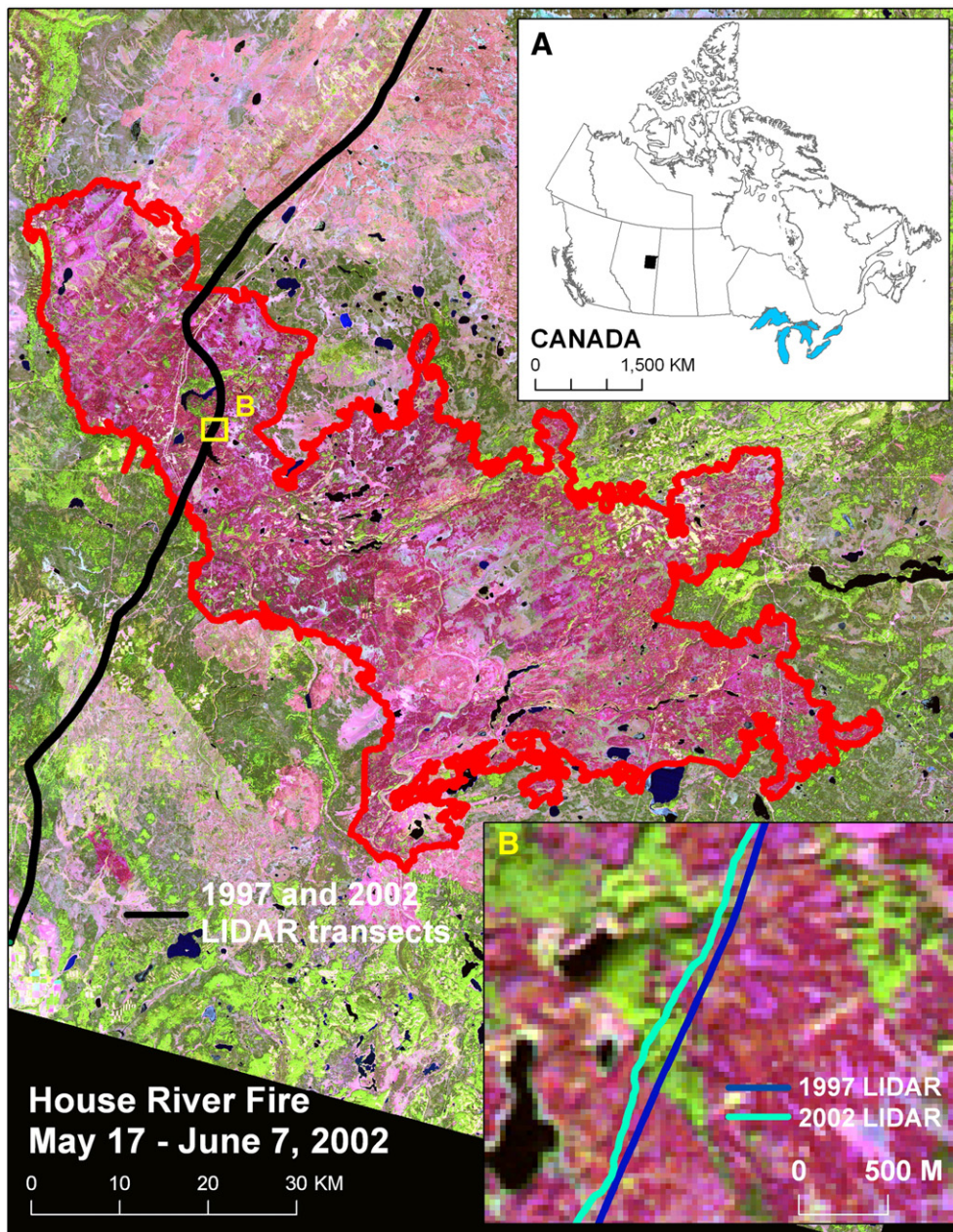
The assessment of post-fire effects considers ecosystem conditions prior to the fire, and the amount of aboveground vegetation and forest floor fuel consumed by the fire. Ecosystem conditions prior to the fire are characterized by vegetation type and structure, and by forest floor composition, with the latter being influenced by soil type, depth, bulk density, and inorganic content. The amount of fuel consumed (aboveground vegetation and forest floor) is dependent on fuel characteristics such as fuel load, bulk density, horizontal and vertical distribution of vegetation, fuel moisture, and weather. Wildfires are typically more severe when temperatures, wind speeds, and fuel loads are high, and humidity and fuel moisture are low. Post-fire effects can differ for aboveground vegetation and soil/forest floor. In boreal forests, a low intensity surface fire can create high soil/forest floor burn severity if a large amount of surface fuels have accumulated and are consumed, while a high intensity crown fire in an area with moist soil/forest floor conditions can lead to a high aboveground burn severity, but to a low soil/forest floor burn severity (DeBano et al., 1998; Dahlberg, 2002; Graham et al., 2004). Thus different soil surface burn severity levels can occur in combination with different aboveground vegetation burn severity levels, rendering the application of a composite burn severity index challenging under certain conditions (Kasischke et al., 2008).

Forest structural attributes such as canopy bulk density and canopy base height are associated with aboveground vegetation burn severity. Tree canopy base height has been highlighted as one of the most important factors for crown fire initiation in conifer forests in the inland western United States (Jain & Graham, 2007). Information on vertical forest structure is therefore important when studying aboveground burn severity, because vertical continuity and bulk density of fuels from the ground to the crown increases the likelihood of crown fire occurrence and spread rate, respectively (Monleon et al., 2004); however, high canopy bulk densities and low canopy base heights alone do not necessarily lead to a fast spreading crown fire with a high aboveground burn severity (Hall & Burke, 2006).

Mapping of post-fire effects is necessary for management of post-fire recovery and timber salvage (Miller & Yool, 2002) and aids in predicting and understanding rehabilitation and succession processes (Turner et al., 1998). Assessment of post-fire effects in the field is a subjective process using tools such as the Composite Burn Index (CBI) field protocol (Key & Benson, 2006) which was designed to be correlated with remotely sensed estimates of burn severity (Lentile et al., 2006a). The CBI protocol is used to calibrate and validate burn severity maps produced from remotely sensed data (Hall et al., 2008; Key & Benson, 2006) and assesses average post-fire effects (quantity of fuel consumed, degree of soil charring, degree of vegetation rejuvenation) over a square 30 m by 30 m plot, which is then matched to the severity measured from remotely sensed data. Burn severity is typically classified into broad damage classes (e.g., low, moderate, high) (Diaz-Delgado et al., 2004; DeBano et al., 1998; Isaev et al., 2002; Mitri & Gitas, 2008; Patterson & Yool, 1998; Robichaud, 2000), although there is an important variation in these classifications across regions and vegetation types (Lentile et al., 2006a). Assessment of post-fire effects using remotely sensed data are dependent on spatial, temporal, and radiometric considerations, and the complex interactions of these factors (Key, 2006).

2.2. Normalized Burn Ratio (NBR), delta NBR (dNBR), and Relative dNBR (RdNBR)

A wide variety of remotely sensed data sources have been used to map areas impacted by fire at regional (Röder et al., 2008), national (Goetz et al., 2006), continental (Masek et al., 2008; Pu et al., 2007), and

Fig. 1. Study area and perimeter of the House River fire. The post-fire Landsat Thematic Mapper image was acquired on September 11, 2002 (shown as a standard band 5, 4, 3 composite). The LIDAR data was acquired in September 1997 (pre-fire) and September 2002 (post-fire).

global scales (Chuvieco & Martin, 1994; Giglio et al., 2005, 2006; Roy et al., 2005). Remotely sensed data have also been proposed for capturing the variability in fire severity within burn perimeters (Duffy et al., 2007; Epting et al., 2005; Mitri & Gitas, 2008; Robichaud et al., 2007; van Wagtendonk et al., 2004; White et al., 1996), as well as post-fire recovery (Diaz-Delgado et al., 2004; Henry & Hope, 1998; Röder et al., 2008; Viedma et al., 1997; van Leeuwen, 2008). Operationally, satellite-derived maps of burn severity are generated by the Burned Area Emergency Response (BAER) Imagery Support program, and these products, the Burned Area Reflectance Classification (BARC), are generated primarily from the dNBR and are used as inputs for final severity maps (Safford et al., 2008).

Key and Benson (2006) introduced the use of a scaled spectral index, the Normalized Burn Ratio (NBR), to map burn severity using Landsat TM/ETM+ data. The NBR is calculated using TM/ETM+ bands 4 and 7, each of which have differing spectral responses to fires (Miller & Yool, 2002). Band 4 is sensitive to chlorophyll content in live vegetation and spans the electromagnetic wavelengths in the near-infrared (0.76–0.90 μm), while band 7 is located in the middle-infrared (2.08–2.35 μm) and is sensitive to the water content in vegetation. The NBR is calculated as follows:

$$NBR = (B4 - B7) / (B4 + B7). \tag{1}$$

The NBR has been used to map burn severity in a variety of forest biomes (Cocke et al., 2005, Epting et al., 2005; Lentile et al., 2006a; Miller & Yool, 2002; Stow et al., 2007; van Wagtendonk et al., 2004; Wimberly & Reilly, 2007). The NBR is often used in change detection whereby post-burn NBR is subtracted from the pre-burn NBR to produce a delta Normalized Burn Ratio (dNBR) image:

$$dNBR = (PreFireNBR - PostFireNBR). \tag{2}$$

The dNBR is intended to normalize for spatial variation in pre-fire vegetation cover. Several studies have identified the dNBR as an accurate and repeatable tool for detecting burn severity (Key & Benson, 2006; van Wagtendonk et al., 2004); however, the relationship between dNBR and field measures of severity, specifically the Composite Burn Index (CBI), have been tenuous, particularly in Alaskan boreal forests (Allen & Sorbel, 2008; Epting et al., 2005; Hoy et al., 2008; Murphy et al., 2008). Verbyla et al. (2008) identified phenology and solar elevation as confounding factors to mapping burn severity with the dNBR in high-latitude areas such as Alaska. In other areas (*i.e.*, western Canadian boreal forest), relationships between dNBR and fire severity have been found to be more robust (Hall et al., 2008).

When calculating any multi-temporal index using NBR, the input Landsat data should be corrected to a reflectance standard (top-of-atmosphere (TOA) or surface) to facilitate comparison between multiple image dates. If field measures of burn severity (e.g., CBI) will be used for comparison, the images should be corrected to surface reflectance. Roy et al. (2006) assessed the performance of NBR and dNBR indices over African savannah regions, and concluded that these indices were not optimal for describing fire severity in areas with low amounts of forest cover. Miller and Thode (2007) pointed out that dNBR is strongly correlated with pre-fire green biomass, because areas with the greatest absolute difference between pre- and post-fire vegetation cover will achieve the highest (dNBR) severity values. Therefore, if two areas with different pre-fire cover experience a stand-replacing fire, each could be assigned to a different burn severity class. In this context, Miller and Thode (2007) proposed a relative version of the dNBR (RdNBR) that accounts for variability in pre-fire vegetation density. The RdNBR is calculated as follows:

$$RdNBR = \frac{dNBR}{\sqrt{ABS(prefireNBR / 1000)}} \quad (3)$$

2.3. LIDAR and fire applications

In the context of forest fire mapping and monitoring, LIDAR data have been used primarily to characterize and map forest fire fuels, an important input for forest fire behaviour models. Riaño et al. (2003) developed methods for automatically extracting forest parameters (*i.e.*, tree height, tree cover, surface canopy height, foliage biomass, and crown volume) for fire behaviour modeling from small footprint discrete return LIDAR. These methods were then applied in an intensively managed Scots pine (*Pinus sylvestris* L.) forest in central Spain (Riaño et al., 2004). Plot level estimates of crown volume ($r^2 = 0.92$), and foliage biomass ($r^2 = 0.84$) (used to derive crown bulk density) were found accurate relative to field measurements. Andersen et al. (2005) also used a discrete return small footprint LIDAR and applied a similar approach over a more complex conifer forest in the United States Pacific Northwest to estimate canopy fuel weight, canopy bulk density, canopy base height, and canopy height. Their outputs were used to generate maps of forest fuel distribution that were subsequently input to a forest fire behaviour model. Other studies have also used LIDAR to map forest fuels (Mutlu et al., 2008; Skowronski et al., 2007) grassland fuels (Varga & Asner, 2008), and shrubs (Riaño et al., 2007).

3. Study area

The study area is located in Alberta, Canada (Fig. 1), within the Boreal Plains ecozone, one of 15 terrestrial ecozones in Canada (Marshall & Schut, 1999). The area is characterized by moderate topography, with elevation ranging from 600 to 760 m. White spruce (*Picea glauca*), black spruce (*Picea mariana*), jack pine (*Pinus banksiana*), and tamarack (*Larix laricina*) are the main conifer species in this region. There is also a wide distribution of broadleaf trees,

Table 1
Forest structural attributes derived directly or indirectly from discrete return LIDAR profiling data.

Directly derived attributes	Average canopy height (ACH) (m)
	Vegetation fill at 1 m (VF$_1$) (%)
	Vegetation fill at 2 m (VF$_2$) (%)
	Vegetation fill at 5 m (VF$_5$) (%)
	Vegetation fill at top of canopy (maximum height) (VF$_T$) (%)
	Crown closure (CC) (%)
	Average inter-tree distance (AID) (m)
Indirectly derived attributes	Volume (VOL) (m^3/ha)

particularly white birch (*Betula papyrifera*), trembling aspen (*Populus tremuloides*), and balsam poplar (*Populus balsamifera*). Precipitation is about 400 mm over much of the ecozone, nearing 500 mm along the southern boundary. The mean daily January temperature ranges from − 17.5 °C to − 22.5 °C, with the mean daily July temperature ranging from 12.5 °C to 17.5 °C (Lands Directorate, 1986).

This study focuses on the House River fire, which ignited on May 17, 2002, and burned until June 7, 2002, consuming approximately $343 million worth of merchantable timber over an area of 248,000 ha. The fire was the second largest in Alberta since 1961, and the most expensive in the Province's history, with suppression costs estimated at $49.3 million (Baxter, 2003; Tymstra et al., 2005). The fire was very intense and with the aid of strong southeast winds, the fire traveled more than 70 km and burned in excess of 60,000 ha in the first 3 days. In the six-months preceding the House River fire, the area had experienced prolonged drought, receiving only 56% of its 30-year average precipitation (Tymstra et al., 2005). The perimeter of the fire is shown in Fig. 1.

4. Data

Two Landsat images (Path 42, Row 21) were acquired to represent pre- (August 15, 2001; ETM+) and post-fire (September 11, 2002; TM) conditions for the House River fire. Two LIDAR transects were flown in September 1997 and 2002 (Fig. 1) with an airborne discrete return profiling LIDAR system, composed of an infrared laser altimeter, video camera, and a GPS receiver (Sweda, 1998). Each LIDAR transect collected was approximately 600 km in length (Wulder et al., 2007); however, only a portion of the total transect, approximately 170 km in length, was considered in this study, of which 120 km is located within the perimeter of the House River fire (Fig. 1). The 2002 flight line was deliberately designed to follow the 1997 flight line. Known logistical issues such as flying conditions (e.g. wind, topography) made it challenging to replicate the 1997 flight line, even with GPS guidance (Wulder et al., 2007), resulting in flight lines that are not exactly spatially coincident. The average and median distances between the two flight lines (over their total length) are 98 m and 79 m respectively (Wulder et al., 2007). The average and median distances for the portion of the two flight lines considered in this analysis are: 131 m and 117 m, respectively. This lack of spatial coincidence between the LIDAR transects necessitated an image segmentation stage in our analysis to ensure a spatially consistent comparison over time.

5. Methods

5.1. Pre-processing of Landsat data

The capability of the NBR, dNBR, and RdNBR to characterize post-fire effects depends on several factors, including the timing of pre- and post-fire image acquisition and mitigation of the surface changes that are not attributable to fire (e.g., moisture content, phenology (Key & Benson, 2006)). For this reason, the pre- and post-fire images need to be acquired temporally as close as possible, at least within the same season
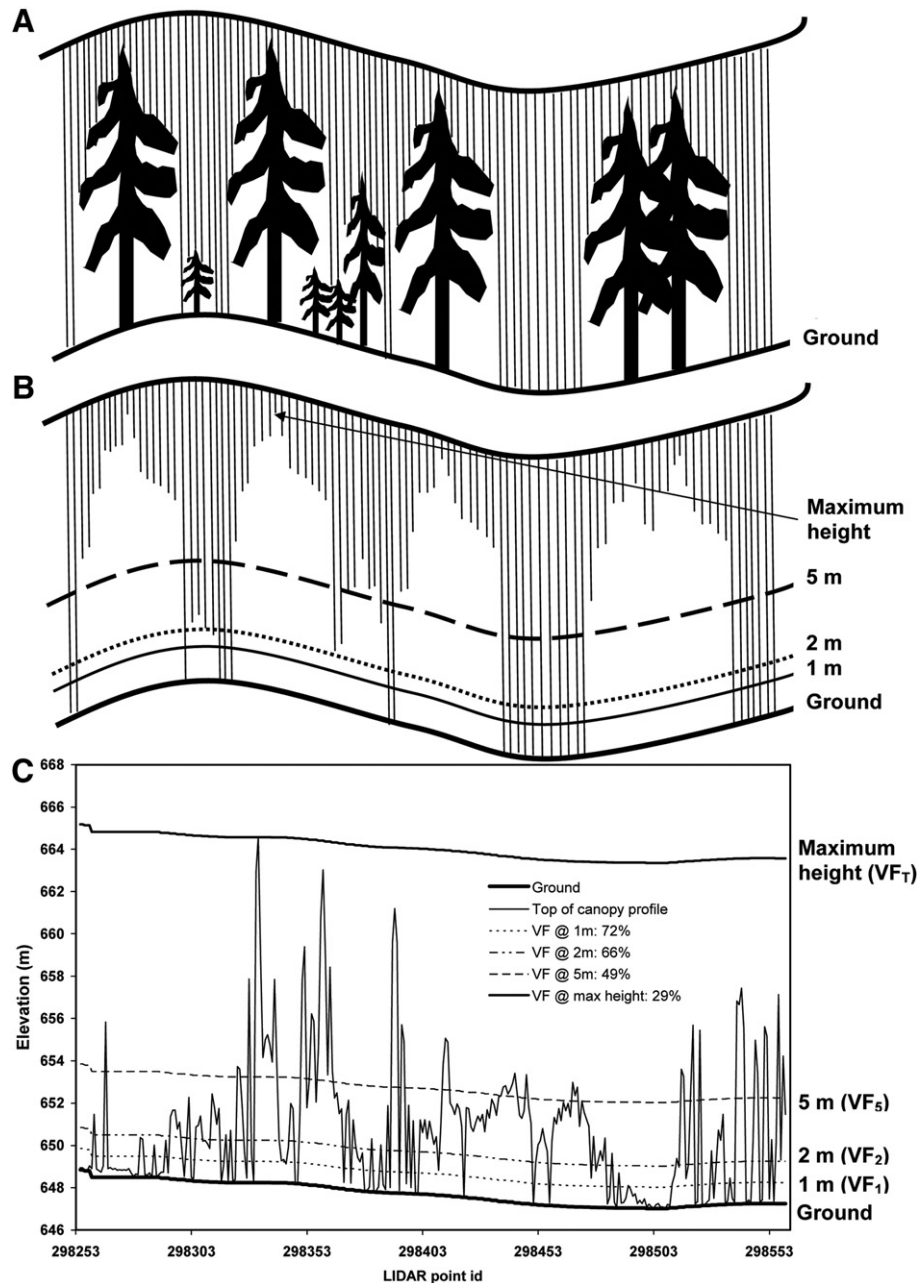
Fig. 2. An illustration of the measurement of vegetation fill using a discrete return profiling LIDAR data.

of the same year or in the same season in a different year. To mitigate differences between the pre- and post-fire images resulting from discrepancies in sensor gain and offset, sun angle, solar irradiance, and between-scene variability, the two Landsat images acquired for this study were first atmospherically corrected (TOA) and normalized to surface reflectance, and then spatially co-registered. The 2001 Landsat ETM+ image was geo-corrected to 1:50,000 Canadian National Topographic System planimetry and road vectors (UTM NAD83 projection) using 25 GCPs, a second order polynomial, and nearest neighbour resampling, resulting in a root mean square error (RMSE) of approximately 22 m. The 2002 TM image was then co-registered to a 2001 image using 30 GCPs, a 2nd order polynomial, and nearest neighbour resampling, yielding an RMSE of approximately 16 m. An efficient image processing approach, similar to that proposed by Han et al. (2007), was employed to streamline the correction and normalization process and avoid errors related to operator intervention and data scaling between processing steps.

5.2. Segmentation of Landsat images

Image segments were generated from the post-fire Landsat data to provide a spatial framework within which the attributes and temporal dynamics of forest structure were estimated from the LIDAR data and compared. The segments serve as a proxy for homogenous units of vegetation (Woodcock & Harward, 1992), which facilitate analysis of the linkage between forest structure as derived using LIDAR data and post-fire effects as measured from the optical remotely sensed imagery. The segments also account for the spatial disparity between the LIDAR transects, as described in Wulder et al. (2007). The Landsat TM image collected on September 11, 2002 was segmented following procedures outlined in Wulder and Seemann (2003) and Wulder et al. (2007). Definiens software (Definiens Imaging GmbH, München, Germany) was used for segmentation with a post-fire Normalized Difference Vegetation Index (NDVI) as input and the following segmentation parameters:

Table 2
Global analysis: A comparison of pre- and post-fire average values for LIDAR-derived attributes grouped by segment location inside and outside the House River fire perimeter ($\alpha = 0.05$).

Lidar attribute	Inside fire perimeter		Outside fire perimeter		t-test	
	$n = 27$		$n = 40$		independent samples	
	Pre-fire (1997)	Post-fire (2002)	Pre-fire (1997)	Post-fire (2002)	Pre-fire (1997)	Post-fire (2002)
					t-value (p)	t-value (p)
ACH (m)	4.81	2.14	4.44	3.27	−0.648 (0.519)	2.579 (**0.012**)
VF_1 (%)	68.96	45.52	66.05	55.53	−1.035 (0.304)	3.420 (**0.001**)
VF_2 (%)	62.33	35.15	59.55	48.83	−0.891 (0.376)	4.560 (**0.000**)
VF_5 (%)	49.74	23.59	47.35	36.83	−0.691 (0.492)	4.458 (**0.000**)
VF_T (%)	22.48	10.81	21.70	17.23	−0.433 (0.666)	4.344 (**0.000**)
CC (%)	52.04	22.22	49.03	39.40	−0.814 (0.418)	5.458 (**0.000**)
AID (m)	7.03	14.47	9.46	6.81	0.675 (0.502)	−2.248 (**0.028**)
VOL (m³/ha)	927.10	539.53	1096.85	890.11	1.063 (0.291)	2.571 (**0.012**)

Significant values are indicated in bold.

scale (5), color (0.9), compactness (0.5), shape (0.3), and smoothness (0.5).

5.3. Calculation of NBR, dNBR, and RdNBR

Although Key (2006) suggested categorizing dNBR values, subsequent studies have indicated that these fixed thresholds of burn severity may not be universally applicable, since the range and distribution of dNBR values are not consistent, even if images are radiometrically corrected and normalized prior to calculating dNBR (Miller & Thode, 2007; Roy et al., 2006). Furthermore, inconsistency in the definition of fire severity classes has led to confusion and conflicting results in the scientific community (Lentile et al., 2007; Odion & Hanson, 2008; Shakesby & Doerr, 2006; Safford et al., 2008). Therefore, in this study we did not use thresholds to categorize NBR, dNBR, or RdNBR values.

To characterize post-fire effects, pre- and post-fire NBR, dNBR, and RdNBR were calculated using Eqs. (1)–(3), and subsequently decomposed (Wulder & Franklin, 2001) to the Landsat-derived image segments. The Windsorized mean value of each burn index was assigned to each segment. The Windsorized mean is a robust estimator of the population mean and is relatively insensitive to outliers; it was computed to reduce the effects of extreme values in the segment (SAS Institute Inc., 2004), and was calculated at a 95% confidence level using 5% of observations Windsorized from the tails of the distribution. The distribution of pre- and post-fire NBR, dNBR, and RdNBR values inside and outside the fire perimeter were compared by means of the non-parametric Mann–Whitney U test (95% confidence level) and histograms of the segment values.

5.4. LIDAR data pre-processing and derivation of forest structural attributes

Before deriving forest structural attributes to characterize fire-caused changes, the LIDAR data were pre-processed to reconcile differences in sampling densities between transects, extract ground elevation profiles, and calculate vegetation height profiles. Further details regarding the LIDAR pre-processing and attribute derivation are described in Wulder et al. (2007). Forest structural attributes (Table 1), were calculated using the LIDAR points within each Landsat-derived segment. Average canopy height (ACH) measures (in metres) the mean height of the canopy in each segment. Volume (VOL) was derived indirectly using empirical relationships between field-based volume measurements and the profile area under the top of the canopy, as per Wulder et al. (2007).

Vegetation fill is a measure derived from the profile area under the canopy. The profile area under the canopy is defined as the cross-sectional area between the top of the canopy profile and the ground surface (Fig. 2A), and is particularly useful as it represents both the height and density of the vegetation (Wulder et al., 2007). The following equation is used to calculate the profile area under the canopy or at a specified height threshold:

$$Area_{profile} = \frac{1}{2} \sum_{i=1}^{n} [s_{i-1} \times (h_{i-1} + h_i)] \qquad (4)$$

where n is the number of LIDAR points; s_i is the distance between LIDAR points i and $i-1$; and h_i is the canopy height at point i. Profile areas under 1, 2, and 5 m height thresholds were likewise generated (Fig. 2B). The total cross-sectional area of the LIDAR profile for any given segment is calculated using the following equation:

$$Area_{cross} = h \times l \qquad (5)$$

where h is the height threshold (1, 2, 5 m, and maximum canopy height) and l is the length of the LIDAR profile within the segment. The ratio of the canopy profile area to the total cross-sectional area for any given height threshold provides an indication of vegetation density by vertical canopy location. This ratio is termed vegetation fill (VF) and indicates what proportion of the total vertical cross-

Table 3
A Mann–Whitney U test was used to compare pre- and post-fire structure attributes and remotely sensed measures by segment, inside ($N = 27$) and outside ($N = 40$) the House River fire perimeter ($\alpha = 0.05$).

Variable	Pre-fire (1997)			Post-fire (2002)			Absolute change (d)			Relative change (R)		
	U	Z	p	U	Z	p	U	Z	p	U	Z	p
ACH (m)	499.0	−0.52	0.605	332.5	2.65	**0.008**	295.0	−3.13	**0.002**	200.0	−4.34	**0.000**
VF_1 (%)	520.5	−0.24	0.808	228.0	3.98	**0.000**	150.5	−4.97	**0.000**	126.0	−5.29	**0.000**
VF_2 (%)	524.5	−0.19	0.848	239.5	3.83	**0.000**	164.0	−4.80	**0.000**	131.0	−5.22	**0.000**
VF_5 (%)	537.0	−0.03	0.975	228.0	3.98	**0.000**	271.5	−3.43	**0.001**	220.0	−4.08	**0.000**
VF_T (%)	498.0	−0.53	0.596	296.5	3.11	**0.002**	193.0	−4.43	**0.000**	189.0	−4.48	**0.000**
CC (%)	527.0	−0.16	0.873	182.5	4.56	**0.000**	111.0	−5.48	**0.000**	88.0	−5.77	**0.000**
AID (m)	420.5	1.52	0.128	397.0	−1.82	0.069	228.0	3.98	**0.000**	206.0	4.26	**0.000**
VOL (m³/ha)	441.0	1.26	0.208	321.0	2.79	**0.005**	433.5	−1.35	0.175	358.0	−2.32	**0.020**
NBR	525.0	−0.19	0.853	0.0	−6.90	**0.000**	0.0	−6.90	**0.000**	1.0	6.88	**0.000**

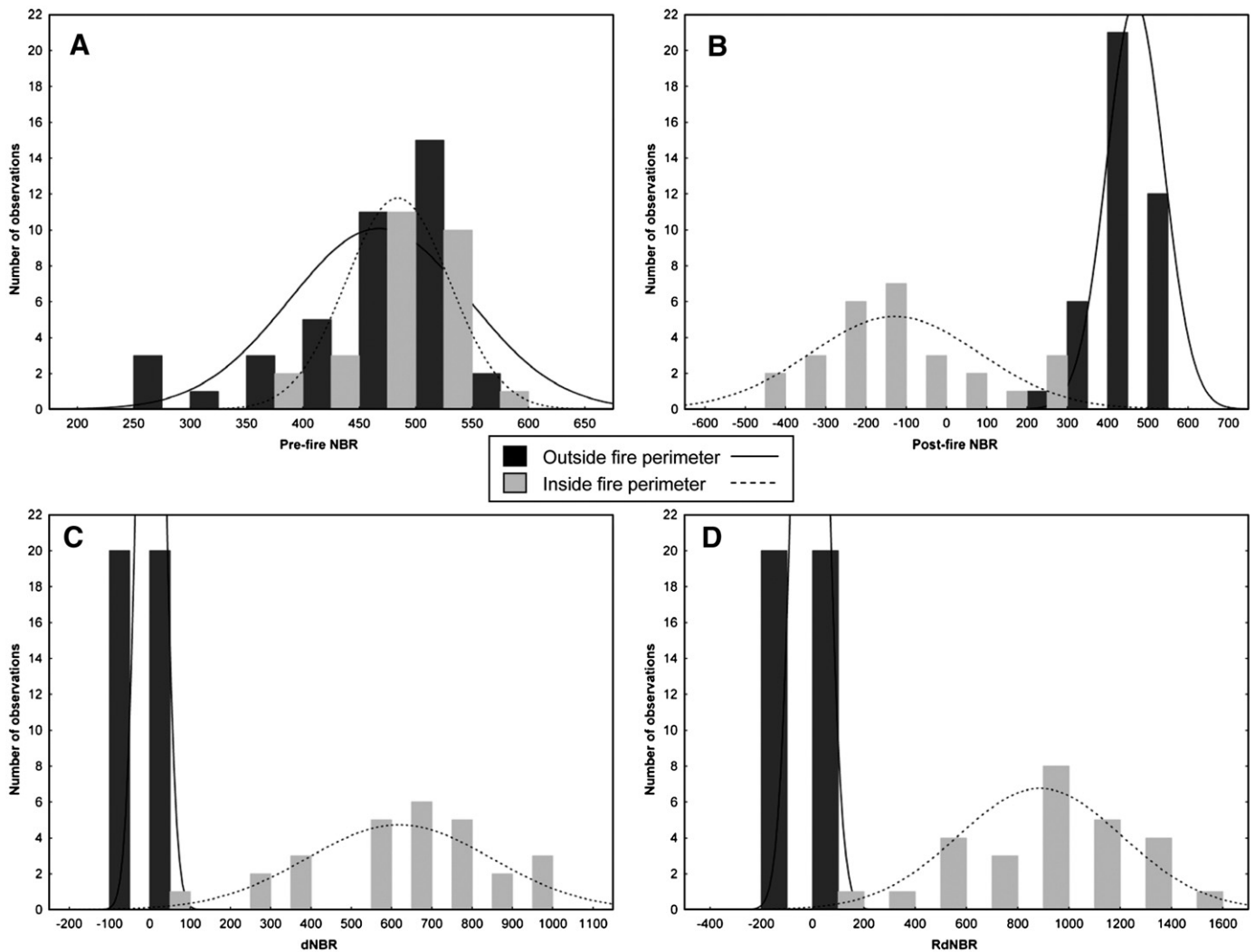Significant values are indicated in bold.

Fig. 3. Pre-fire NBR, post-fire NBR, dNBR, and RdNBR histograms: segments inside and outside the fire perimeter.

sectional area is filled with vegetation. VF is calculated using the following equation:

$$VF_{height} = \frac{Area_{profile}}{Area_{cross}}. \tag{6}$$

In the example shown in Fig. 2C, 29% of the cross-sectional area, as measured from the canopy maximum height, is filled with vegetation, whereas at the 1 m threshold, 72% of the cross-sectional area is filled with vegetation.

Crown closure (CC) and the average inter-tree distance (AID) are additional variables that were not computed in Wulder et al. (2007). CC was estimated as the percentage of LIDAR points within a segment which have a canopy height greater than 2 m. A 2 m height threshold was used to distinguish canopy cover from lower ground cover (Natural Resources Canada, 2004a). AID was generated by calculating the Euclidean distance between consecutive neighbours of points representing individual trees (defined as points with canopy heights greater than 5 m). A 5 m height threshold was used to capture conditions in dominant and sub-dominant strata of the canopy and identifies a minimum height for trees (Lund, 1999; Natural Resources Canada, 2004b).

As per Wulder et al. (2007), forest structural attributes were assessed both globally (for the entire transect) and locally (per segment). The attributes listed in Table 1 were calculated globally by

averaging values for all the segments in the study area that were intersected by both the pre- and post-fire LIDAR transects. The local approach analyzes pairwise segment-based changes in forest structure as a result of the House River fire. An independent sample *t*-test was used to compare values for each of the LIDAR attributes for segments inside and outside the fire perimeter, thereby indicating if there were any significant pre-existing differences between the forests located inside and outside the fire perimeter. The segment-based comparison of pre- and post-fire values evaluated both the absolute and relative changes in attribute values (*x*) as follows:
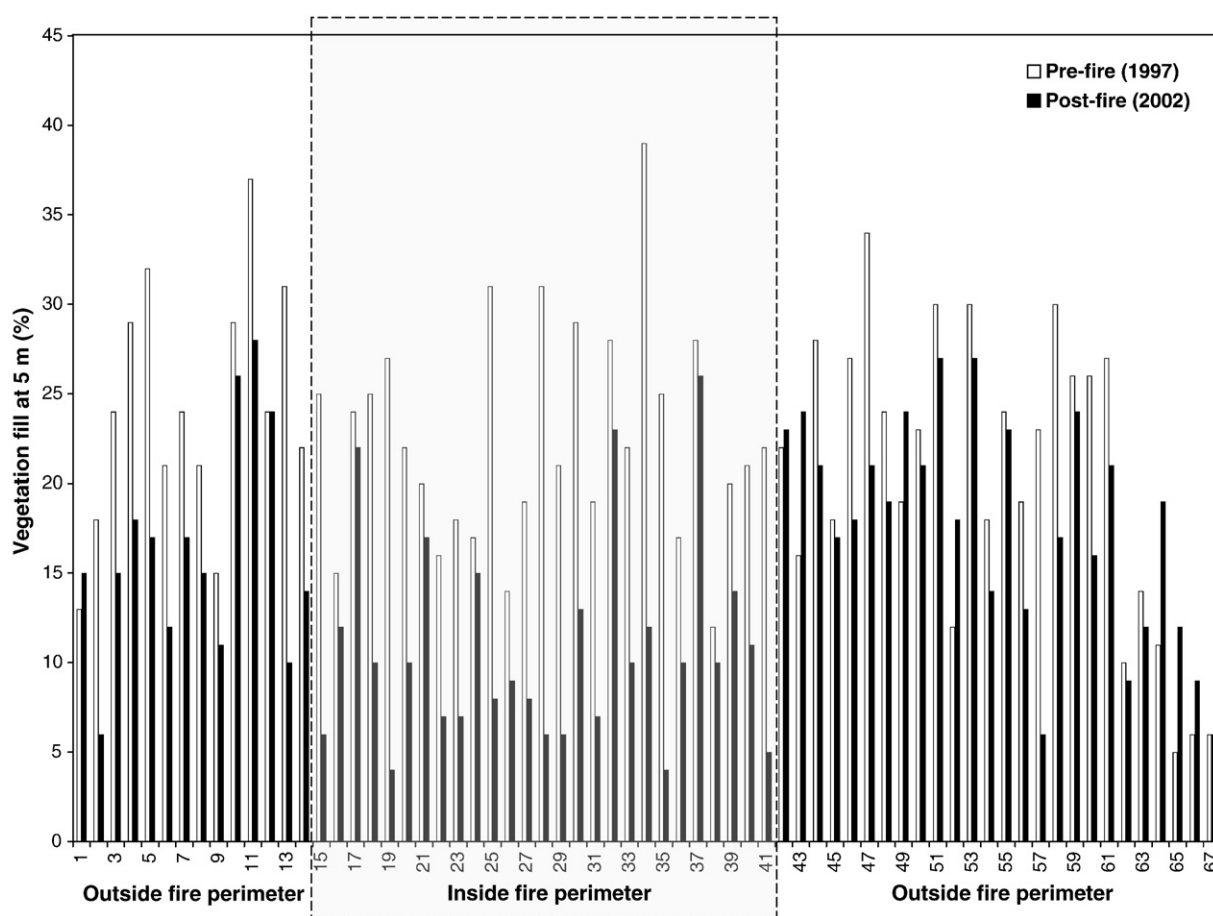
$$dx = PreFire\ x - PostFire\ x \tag{7}$$

$$Rx(\%) = 100\ (PreFire\ x - PostFire\ x)\ /\ PreFire\ x. \tag{8}$$

Forest structural attributes inside and outside the fire perimeter were compared on a segment basis by means of the non-parametric Mann–Whitney *U* test ($\alpha = 0.05$) (Table 2).

5.5. Analysis of changes in forest structure and post-fire effects

The relationships between changes in forest structure (derived from the LIDAR data) and post-fire effects (derived from the Landsat TM images) were analyzed to determine the impact of pre-fire vertical structure on post-fire effects, and to characterize post-fire vertical

Fig. 4. Segment-wise comparison of pre- and post-fire vegetation fill at 5 m (VF$_5$). Segments are plotted in increasing order in the X-axis, following the LIDAR flight direction (from north to south). The location of the fire perimeter relative to the flight path is also shown.

structure and absolute and relative changes in vertical structure in the context of varying fire severity. In the analysis, segments were considered collectively, but given that pre-fire vegetation is posited to have an influence on fire behaviour and therefore on fire severity (Jain & Graham, 2007), the segments were stratified into three classes according to their pre-fire crown closure. Thresholds for crown closure classes were defined according to the Land Cover Classification System used by Canada's National Forest Inventory (Natural Resources Canada, 2004a): >60% for dense forest, 26–60% for open forest, and 10–25% for sparse forest. In addition, the Earth Observation for Sustainable Development of Forests (EOSD) land cover product representing circa 2000 conditions was used to characterize the dominant vegetation type in each segment (Wulder et al., 2003).
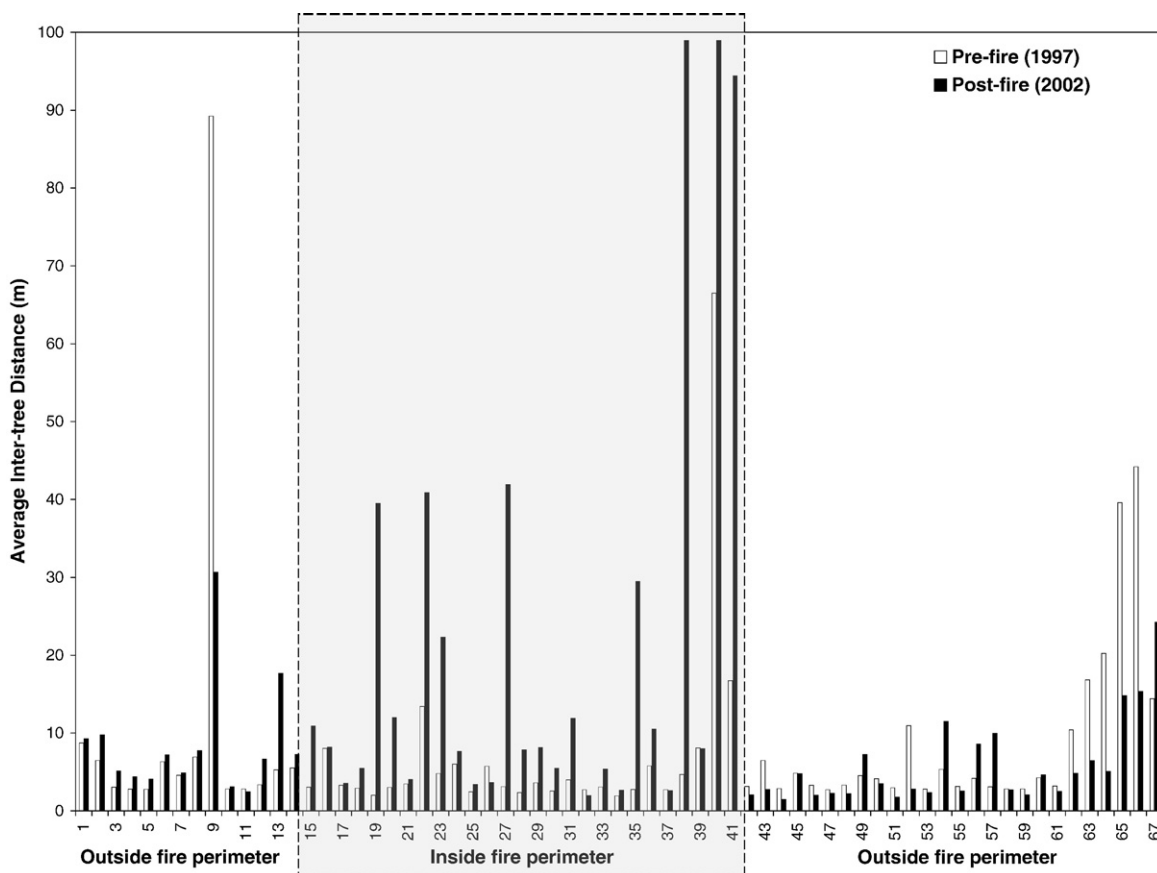
Correlations were calculated between the LIDAR-derived forest attributes (Table 1) and the post-fire NBR, dNBR, and RdNBR (95% confidence level), and simple linear regression analyses were performed for those variables with the highest correlations (as measured by the Pearson *r* coefficient) to explore in more detail the relationship between forest structure and post-fire effects. Segments were also stratified by crown closure. The adjusted R^2 was calculated instead of multiple R^2, to account for the size of the sample. Linear regression assumptions (*i.e.*, independence, homoscedasticity and normality of errors) were tested by residual analysis (*i.e.*, by considering the normal probability plot of raw residuals and plotting the predicted values against the raw residuals).

6. Results

A total of 67 segments generated from the post-fire Landsat image intersected with both the 1997 and 2002 LIDAR transects, with 27 of

these segments located inside the fire perimeter, and 40 segments located outside the fire perimeter. The EOSD land cover indicated that 53 of the 67 segments were coniferous forest, with the remainder being broadleaf, wetland treed, and herbaceous. Table 2 contains a summary of the global averages for the structural attributes stratified by segment location inside or outside the fire perimeter. Pre-fire, there were no significant differences for any of the structural attributes between forests located inside and outside the fire perimeter (Table 2). However, post-fire, there were significant differences for all of the forest structural attributes ($p < 0.05$). This result confirms that observed differences in forest structure post-fire (2002) are primarily attributable to the House River fire, and are not the result of some pre-existing differences between forests located inside and outside the fire perimeter. In addition, we used independent sample *t*-tests to compare the magnitude of the global absolute differences (*i.e.*, pre-fire versus post-fire) inside the fire perimeter to the magnitude of the global absolute differences outside the fire perimeter. The results of these tests (not shown) indicate that for all of the LIDAR-derived attributes listed in Table 2, the differences between pre- and post-fire measures inside the fire perimeter are significantly greater than the differences outside the fire perimeter ($p < 0.05$).

Per-segment comparisons of forests located inside and outside of the fire perimeter (Table 3) indicated that pre-fire, there were no significant differences in any structural attributes or in the NBR, corroborating the results of the global analysis. Post-fire, there were significant differences between forests inside and outside the fire perimeter for all attributes, with the exception of AID. When the absolute change in attributes was considered, VOL was the only attribute for which there was no significant difference. Finally, when relative change was considered (accounting for pre-existing forest

Fig. 5. Comparison of pre- and post-fire average inter-tree distance (AID). Segments are plotted in increasing order in the *X*-axis, following the LIDAR flight direction (from north to south). The location of the fire perimeter relative to the flight path is also shown.

condition), significant differences between forests inside and outside of the fire perimeter were found for all the forest structural attributes considered (Table 3). The post-fire NBR, dNBR, and RdNBR inside the fire perimeter were significantly different from the post-fire NBR, dNBR, and RdNBR outside the fire perimeter ($p<0.0001$) (Table 3). The distributions of the pre-fire NBR values indicate the similarity of forests inside and outside the fire perimeter (Fig. 3A). The histograms of post-fire NBR, dNBR, and RdNBR fit a bimodal distribution, indicative of the differences between forests inside and outside of the fire perimeter after the House River fire (Fig. 3B–D).

Fig. 4 shows the segment-based absolute differences in vegetation fill at 5 m (VF_5), following the LIDAR flight path through the fire perimeter, traveling from the NE (segment 1) to the SW (segment 67), with the relative location of the fire perimeter indicated on the x-axis. From 1997 to 2002, segments outside the fire experience both increases and decreases in VF_5; however, inside the fire perimeter, VF_5 does not increase, and on average, decreases in VF_5 inside the fire perimeter are larger than those outside the fire: VF_5 decreased by an average of 4.48% (SE = 1.07%) outside the fire perimeter, while the mean decrease in VF_5 inside the fire perimeter was 11.67% (SE = 1.49%). As shown in Tables 2 and 3, differences between pre- and post-fire values for VF_5 are statistically significant, when compared globally inside and outside the fire, and when compared locally by segment (including both absolute and relative change in VF_5). Similar trends are found for the other measures of vegetation fill (at top of canopy, and 1 and 2 m above ground).

Absolute and relative segment-level changes in AID were significant (Table 3) and are shown in Fig. 5. On a segment basis, AID decreased (absolute difference) by an average of 2.65 m (SE = 1.86 m) outside the fire perimeter, and increased (absolute difference) by an average of 12.79 m (SE = 3.96 m) inside the fire perimeter. In Fig. 6, we

illustrate how such a difference in AID may occur. First, trees must be greater than 5 m in height in order to be included in the calculation of AID, so trees that were less than 5 m in 1997 would not have been included in the calculation of pre-fire AID (Fig. 6A). Inside the fire perimeter, portions of crown foliage would be consumed by fire, resulting in less surface area to intercept the LIDAR pulses (Fig. 6B), contributing to an increase in AID. With portions of the crown consumed by fire, the highest point of the crown, as measured by the LIDAR, may now be in a different location on the crown (Fig. 6B), which also contributes to a difference in AID. Furthermore, if portions of crown foliage corresponding to the LIDAR profile have been consumed, the LIDAR profile may no longer intersect a crown, also contributing to a difference in AID (Fig. 6B). Outside the fire perimeter, trees that were less than 5 m in height in 1997 may exceed the 5 m threshold by 2002 and would have been included in the AID calculation in 2002, resulting in a decrease in AID (Fig. 6C). Average decreases in inter-tree distance outside the fire perimeter are expected, as tree crowns grow over time and increase in size. Large decreases in inter-tree distance outside the fire perimeter (e.g., segment 9, Fig. 5) on a segment-specific basis are more difficult to explain and may be exceptions to the dominant trends present.

Fig. 7 illustrates the segment-level changes in crown closure. Outside the fire perimeter, CC decreased by an average of 9.6% (SE = 1.83%), and inside the fire perimeter, CC decreased by an average of 29.87% (SE = 2.48%). This large increase in CC inside the fire perimeter may be attributed to the fire's consumption of portions of tree crowns, resulting in less surface area to intercept the LIDAR pulses. Since CC is estimated as the percentage of LIDAR returns within a segment that have a height greater than 2 m, when there is less vegetation and therefore fewer LIDAR returns, the CC can change considerably. Global analysis indicated that pre-fire, there was no
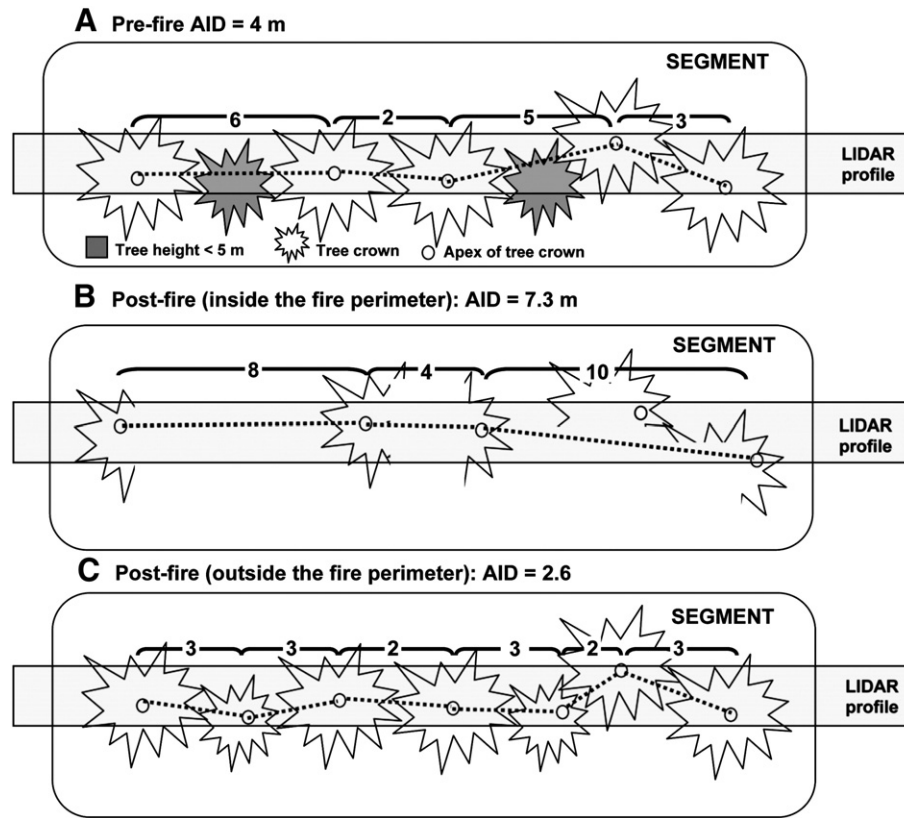
Fig. 6. An example of the estimation of AID (A) pre-fire, (B) post-fire inside the fire perimeter, and (C) post-fire outside the fire perimeter.

significant difference in CC inside and outside the fire perimeter. Post-fire, there was a significant difference in crown closure inside and outside the fire perimeter (Table 2). On a per segment basis, there was a significant difference in post-fire crown closure and in the absolute and relative changes in crown closure.

Inside the fire perimeter, the mean absolute decrease in ACH was 2.7 m (SE = 0.38 m), while outside the fire perimeter, the mean absolute decrease in ACH was 1.16 m (SE = 0.23 m). Mean relative changes in ACH were 54.3% (SE = 4.5%) inside the fire perimeter and 20.5% (SE = 4.9%) outside the fire perimeter. As noted for AID and VF, the ACH is not actually decreasing, but rather that the fire's consumption of portions of the canopy has resulted in less surface area to intercept the LIDAR pulses and thereby impacted the calculation of the ACH value. Outside the fire perimeter, the smaller decrease in ACH is attributable to the nature of profiling LIDAR measures: the 2002 LIDAR profile is not perfectly spatially coincident with the original 1997 LIDAR profile, and therefore different areas of the canopy (within the same segment) are captured in each. Depending on where the profiles are found relative to the configuration of the forest canopy, differences in structural estimates are expected between the two profiles.

Correlations between post-fire effects, as measured by post-fire NBR, dNBR, and RdNBR, and the post-fire, and absolute and relative changes in forest structural attributes derived from the LIDAR data, are summarized in Table 4. These correlations varied in direction, strength, and significance. Forest structural attributes generated from the post-fire 2002 LIDAR transect were most strongly positively correlated to post-fire NBR, while dNBR and RdNBR had stronger positive correlations with absolute and relative changes in the forest structural attributes. Absolute and relative changes in VF and changes in CC had the strongest positive correlations with respect to dNBR and RdNBR, with R-values ranging between 0.514 and 0.715 (p<0.05). No significant correlations were found between post-fire NBR, dNBR, RdNBR and the pre-fire forest

structural attributes (not shown). Relative changes in ACH were significantly negatively correlated with post-fire NBR, and significantly positively correlated to both dNBR and RdNBR. Post-fire CC was significantly negatively correlated to both dNBR and RdNBR, and significantly positively correlated to post-fire NBR. The absolute change in CC was significantly negatively correlated to post-fire NBR and significantly positively correlated to dNBR and RdNBR. Correlations between AID or VOL and the post-fire NBR, dNBR, and RdNBR were weak and not significant.

Based on the strength of their correlations, relationships between post-fire NBR, dNBR, and RdNBR indices and VF at different heights, ACH, and CC were further analyzed through linear regression. Table 5 shows the results of the linear fitting for all segments combined (n = 67), and dense (n = 18) and open forests (n = 42). None of the adjusted R^2 values for open forests were >0.50, and no significant correlations were found in sparse forests (n = 7, not shown). For all segments combined, the strongest fit was between absolute change in CC and dNBR (adjusted R^2 = 0.502, p<0.001) and absolute change in CC and RdNBR (adjusted R^2 = 0.503, p<0.001). For dense forests, the best fit was with absolute change in vegetation fill at the top of the canopy (VF_T) and post-fire NBR (0.894, p<0.001) (Table 5). The suitability of model fit was verified by plotting the line of best fit and the 95% confidence interval bands, as well as the normal probability plot and raw residual for the model. Another interesting result of this work is that although the adjusted R^2 values for all of the severity indices were similar in magnitude, the post-fire NBR R^2 values were consistently larger than those of dNBR and RdNBR for all LIDAR attributes with the exception of VF_5. Fig. 8 illustrates an example of this for post-fire NBR and absolute change in VF_T, with confidence intervals close to the line of best fit, and residual values normally distributed.

Fig. 9 shows the mean and standard deviation for dense and open forests inside and outside the fire perimeter for dNBR and relative change in CC. From this, the difference in dNBR values inside and outside the fire perimeter is apparent, as are the similarity in values for
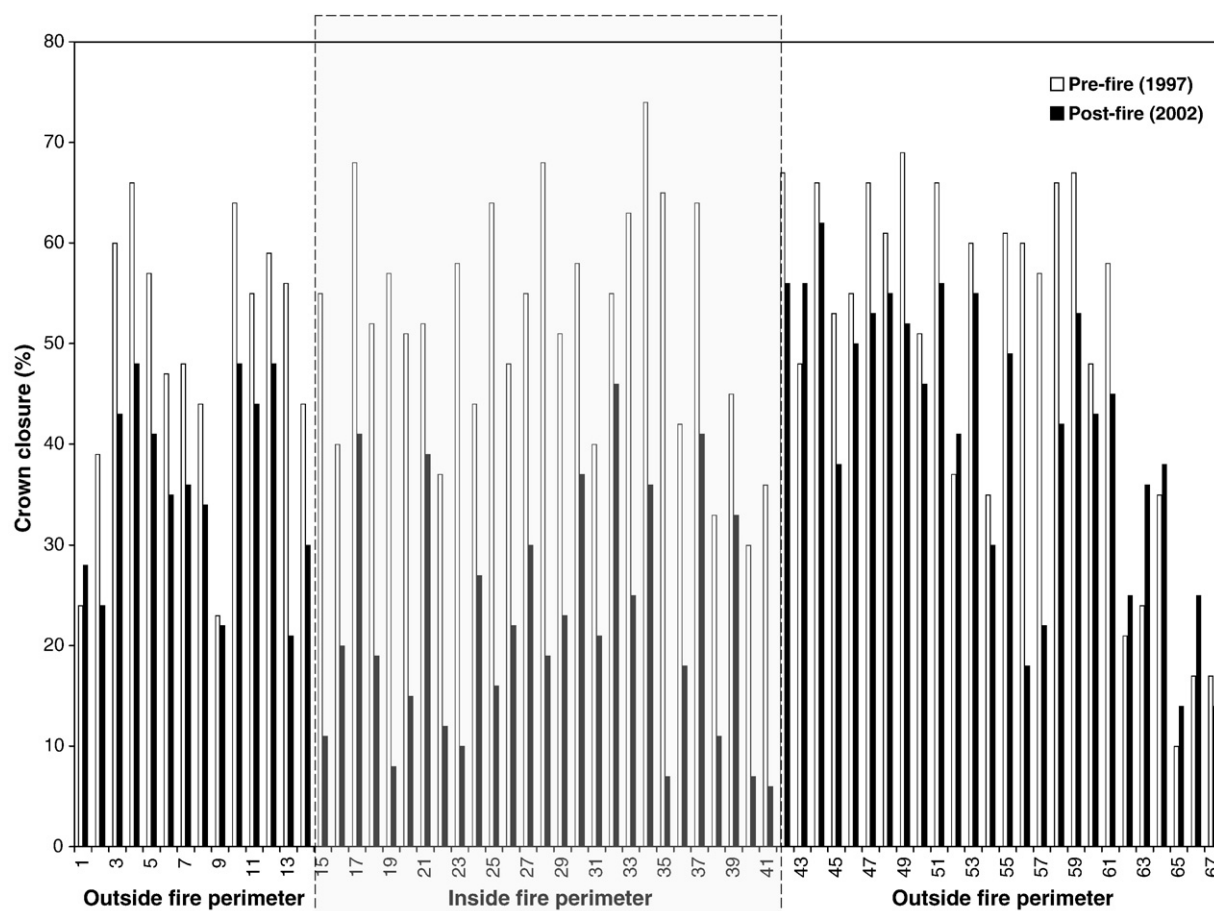
Fig. 7. Segment-wise comparison of pre- and post-fire crown closure. X-axis shows segments following the LIDAR flight direction (from north to south). The location of the fire perimeter is also plotted.

segments dominated by dense and open forests. The relative change in CC for dense and open forests provides an example of why the relationships for this structural attribute are strong and significant for dense forests (Table 5), which have a statistical separation inside and outside the fire perimeter, but not for open forests. Similar trends exist for the other structural attributes considered in the analysis.

7. Discussion

The LIDAR transects used in this study were collected for a more general study of boreal forest depletion and growth (Wulder et al.,

2007), so the spatial correspondence of the transects with the House River fire is fortuitous, and provides a unique opportunity to characterize forest vertical structure before and after a major fire event, and relate these changes in forest structure to measures of post-fire effects generated from optical satellite remotely sensed data. Forest structure is believed to have a role in determining post-fire effects and burn severity, and knowledge of burn severity relative to pre-fire conditions informs fuel management and restoration treatments. However, the results of this analysis indicate that none of the LIDAR-derived measures of pre-fire forest structure generated from the LIDAR data were significantly correlated to the remotely sensed measures of fire severity

Table 4
Correlation between remotely sensed burn severity indices and forest structure attributes derived from the LIDAR data ($n = 67$; in bold: correlations with Pearson's $r > 0.50$, $\alpha = 0.05$).

Variable	Post-fire (2002)			Absolute change (d)			Relative change (R)		
	Post-fire NBR	dNBR	RdNBR	Post-fire NBR	dNBR	RdNBR	Post-fire NBR	dNBR	RdNBR
ACH (m)	0.423	−0.339	−0.334	−0.447	0.479	0.476	**−0.534**	**0.550**	**0.555**
	$p < 0.0001$	$p = 0.005$	$p = 0.006$	$p < 0.0001$	$p < 0.0001$	$p < 0.0001$	$p < 0.0001$	$p < 0.0001$	$p < 0.0001$
VF$_1$ (%)	**0.611**	**−0.531**	**−0.524**	**−0.646**	**0.673**	**0.673**	**−0.661**	**0.673**	**0.675**
	$p < 0.0001$	$p < 0.0001$	$p < 0.0001$	$p < 0.0001$	$p < 0.0001$	$p < 0.0001$	$p < 0.0001$	$p < 0.0001$	$p < 0.0001$
VF$_2$ (%)	**0.595**	**−0.507**	**−0.501**	**−0.620**	**0.657**	**0.656**	−0.437	**0.512**	**0.529**
	$p < 0.0001$	$p < 0.0001$	$p < 0.0001$	$p < 0.0001$	$p < 0.0001$	$p < 0.0001$	$p < 0.0001$	$p < 0.0001$	$p < 0.0001$
VF$_5$ (%)	**0.591**	**−0.519**	**−0.514**	−0.452	**0.514**	**0.519**	**−0.660**	**0.701**	**0.712**
	$p < 0.0001$	$p < 0.0001$	$p < 0.0001$	$p < 0.0001$	$p < 0.0001$	$p < 0.0001$	$p < 0.0001$	$p < 0.0001$	$p < 0.0001$
VF$_T$ (%)	**0.516**	−0.442	−0.435	**−0.601**	**0.620**	**0.617**	**−0.602**	**0.603**	**0.601**
	$p < 0.0001$	$p < 0.0001$	$p < 0.0001$	$p < 0.0001$	$p < 0.0001$	$p < 0.0001$	$p < 0.0001$	$p < 0.0001$	$p < 0.0001$
CC (%)	**0.672**	**−0.589**	**−0.582**	**−0.673**	**0.714**	**0.715**	−0.254	0.267	0.277
	$p < 0.0001$	$p < 0.0001$	$p < 0.0001$	$p < 0.0001$	$p < 0.0001$	$p < 0.0001$	$p = 0.038$	$p = 0.029$	$p = 0.023$
AID (m)	−0.357	0.312	0.320	0.360	−0.353	−0.368	0.469	−0.460	−0.464
	$p = 0.005$	$p = 0.014$	$p = 0.012$	$p = 0.003$	$p = 0.003$	$p = 0.002$	$p < 0.0001$	$p < 0.0001$	$p < 0.0001$
VOL (m³/ha)	0.366	−0.320	−0.317	−0.214	0.217	0.214	−0.254	0.267	0.277
	$p = 0.002$	$p = 0.008$	$p = 0.009$	$p = 0.082$	$p = 0.077$	$p = 0.081$	$p = 0.038$	$p = 0.029$	$p = 0.023$

Table 5
Linear regression between spectral indices and forest attributes derived from the LIDAR data (in bold: adjusted $R^2 > 0.50$, α = 0.05).

		All data (n = 67)						Dense forests (canopy closure > 60%) (n = 18)						Open forests (canopy closure 26–60%) (n = 42)					
		Post-fire NBR		dNBR		RdNBR		Post-fire NBR		dNBR		RdNBR		Post-fire NBR		dNBR		RdNBR	
		Adj-R^2	p	Adj-R^2	p	Adj-R^2	p	Adj-R^2	p	Adj-R^2	p	Adj-R^2	p	Adj-R^2	p	Adj-R^2	p	Adj-R^2	p
Post-fire	ACH	0.167	0.000	0.101	0.005	0.098	0.006	0.394	0.003	0.385	0.004	0.388	0.003	0.153	0.006	0.111	0.018	0.113	0.017
	VF_1	0.363	0.000	0.270	0.000	0.263	0.000	**0.852**	0.000	**0.835**	0.000	**0.831**	0.00	0.345	0.000	0.301	0.000	0.307	0.000
	VF_2	0.344	0.000	0.246	0.000	0.239	0.000	**0.785**	0.000	**0.768**	0.000	**0.765**	0.000	0.348	0.000	0.293	0.000	0.301	0.000
	VF_5	0.339	0.000	0.259	0.000	0.253	0.000	**0.643**	0.000	**0.644**	0.000	**0.645**	0.000	0.314	0.000	0.273	0.000	0.278	0.000
	VF_T	0.255	0.000	0.183	0.000	0.177	0.000	**0.796**	0.000	**0.777**	0.000	**0.773**	0.000	0.230	0.001	0.205	0.002	0.211	0.001
	CC	0.443	0.000	0.337	0.000	0.329	0.000	**0.874**	0.000	**0.858**	0.000	**0.855**	0.000	0.430	0.000	0.369	0.000	0.375	0.000
Absolute change	ACH	0.187	0.000	0.218	0.000	0.214	0.000	**0.684**	0.000	**0.673**	0.000	**0.673**	0.000	0.036	0.121	0.029	0.145	0.028	0.149
	VF_1	0.408	0.000	0.444	0.000	0.444	0.000	**0.893**	0.000	**0.880**	0.000	**0.878**	0.000	0.290	0.000	0.272	0.000	0.270	0.000
	VF_2	0.374	0.000	0.422	0.000	0.421	0.000	**0.783**	0.000	**0.771**	0.000	**0.770**	0.000	0.261	0.000	0.256	0.000	0.254	0.000
	VF_5	0.192	0.000	0.253	0.000	0.258	0.000	**0.505**	0.001	**0.516**	0.000	**0.519**	0.000	0.065	0.056	0.085	0.034	0.087	0.032
	VF_T	0.351	0.000	0.375	0.000	0.372	0.000	**0.894**	0.000	**0.880**	0.000	**0.879**	0.000	0.219	0.001	0.206	0.001	0.204	0.002
	CC	0.445	0.000	**0.502**	0.000	**0.503**	0.000	**0.877**	0.000	**0.860**	0.000	**0.859**	0.000	0.371	0.000	0.356	0.000	0.353	0.000
Relative change	ACH	0.274	0.000	0.292	0.000	0.297	0.000	**0.638**	0.000	**0.619**	0.000	**0.618**	0.000	0.160	0.005	0.145	0.007	0.150	0.007
	VF_1	0.429	0.000	0.444	0.000	0.448	0.000	**0.888**	0.000	**0.875**	0.000	**0.872**	0.000	0.330	0.000	0.306	0.000	0.309	0.000
	VF_2	0.418	0.000	0.440	0.000	0.448	0.000	**0.794**	0.000	**0.782**	0.001	**0.779**	0.000	0.328	0.000	0.311	0.000	0.318	0.000
	VF_5	0.179	0.000	0.251	0.000	0.269	0.000	**0.546**	0.000	**0.560**	0.000	**0.561**	0.000	0.124	0.013	0.147	0.007	0.155	0.006
	VF_T	0.352	0.000	0.354	0.000	0.352	0.000	**0.879**	0.000	**0.865**	0.000	**0.862**	0.000	0.241	0.001	0.226	0.001	0.227	0.001
	CC	0.426	0.000	0.484	0.000	0.499	0.000	**0.877**	0.000	**0.862**	0.000	**0.859**	0.000	0.428	0.000	0.399	0.000	0.406	0.000

Models fitted separately for all data, dense forests, and open forests. Significant correlations were not found in sparse forests.

at this particular site. This suggests that either the LIDAR data are not measuring the structural attributes that impacted this particular fire, and/or that factors other than forest structure played a more important role in determining post-fire effects at this site. Jain and Graham (2007) note that forest structure is only one of the many factors (e.g., weather, vegetation type and moisture, topography) that potentially contribute to variation in post-fire effects (Jain & Graham, 2007).
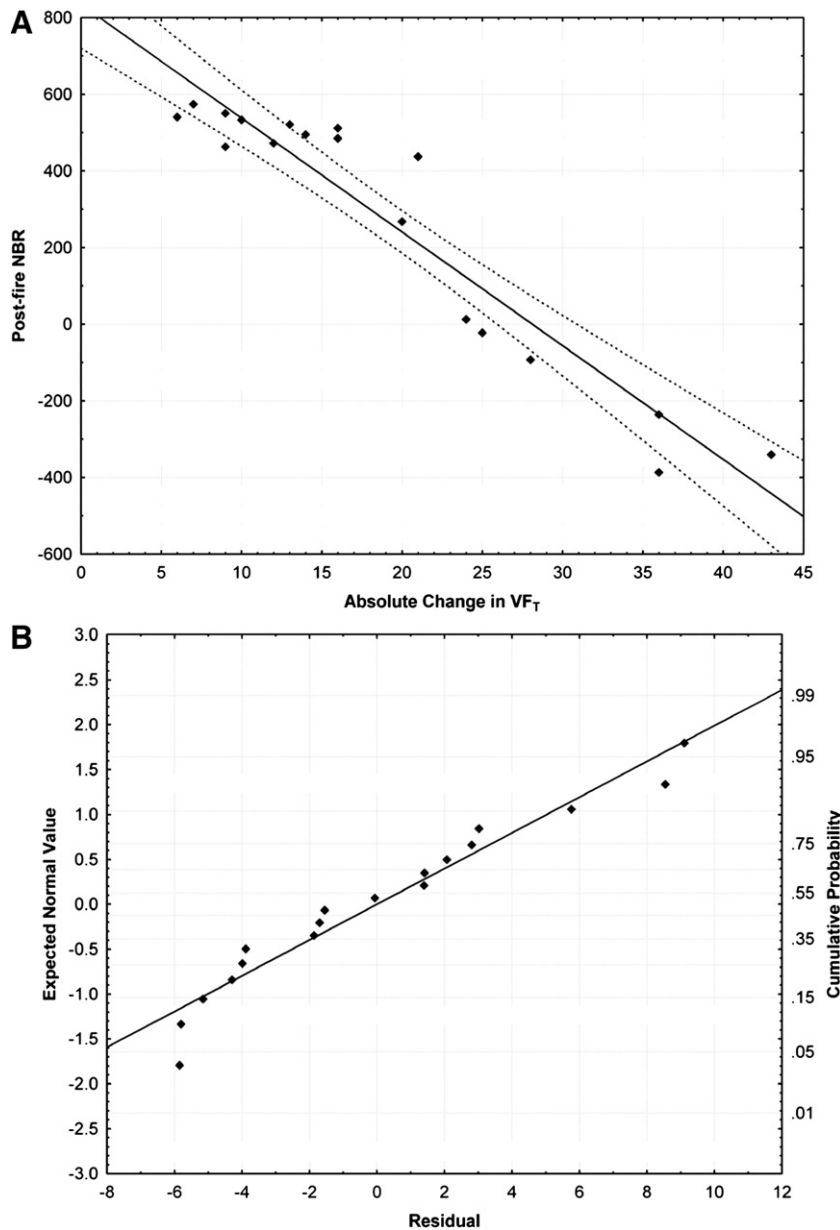
Many studies have identified a linkage between pre-fire forest structure and post-fire effects. For example, Jain and Graham (2007) predicted tree crown burn severity as a function of pre-fire forest structure with probabilities greater than would have occurred randomly, although forest characteristics could not fully explain all the variation in burn severity. Lentile et al. (2006b) found that denser stands with larger trees or many small trees were more likely to have a higher burn severity, and Kuenzi et al. (2008) similarly found that areas of high burn severity were characterized by higher pre-fire plant canopy cover. Other studies have associated tree density, basal area, snag density, and fine fuel accumulation with fire severity (Cocke et al., 2005; Lezberg et al., 2008). In our study area, which was relatively homogenous and dominated by open coniferous forest, we found no significant correlations between post-fire NBR, dNBR, RdNBR and the pre-fire forest structure attributes listed in Table 1.

Remotely sensed data can be used to quickly assess post-fire effects over large areas. Large wildfires leave a mosaic of burn severities and unburned vegetation, and forest managers often strategically prioritize large areas of high burn severity for rehabilitation (Lentile et al., 2007). The heterogeneous nature of post-fire effects has been identified in many studies (Key 2005, 2006; Odion & Hanson, 2006). In the area of the House River fire traversed by the LIDAR transects, there is a marked difference between pre- and post-fire structure in the forests within the fire perimeter. These differences include reduced ACH, decreased VF (measured at maximum height, 5, 2, and 1 m), diminished crown closure, and increased AID. Examples of the heterogeneity in the spatial distribution of these changes in structure are apparent in Figs. 4–6.

One of the major criticisms of remotely sensed estimates of post-fire effects is that linear models used to determine relationships between remotely sensed and field measures of burn severity are data and site specific and therefore cannot be extrapolated to other sites with different cover types and conditions (De Santis & Chuvieco, 2007). Ideally, the relationship between field and remotely sensed measures of burn severity would hold over a range of cover types and conditions and would thereby be applicable over large areas. In an operational context,

the consistency of these relationships is critical, since the primary motivation for using remotely sensed data is the lower cost and large area coverage afforded by this data source, relative to site specific and expensive field surveys. A recent study used a non-linear model to describe the relationship between field-based CBI and dNBR for three separate fires in three different ecozones and ecoregions of the western boreal forest of Canada (Hall et al., 2008). The authors conclude that the relationship between CBI and dNBR may be consistent across a range of ecoregions within the western Canadian boreal forest, suggesting the possibility of a single model for CBI-dNBR in this area. Hall et al. (2008) also suggest that stratifying by pre-burn vegetation condition may further improve modeling of burn severity. Jia et al. (2006) similarly suggested that characterization of forest fuel types with high spatial resolution remotely sensed data may also improve modeling of burn severity. This highlights a potential role for LIDAR in strengthening the link between severity and field measures. Our results identified no significant relationship between any of the pre-fire structural attributes and post-fire NBR, dNBR, or RdNBR. This suggests that additional information on vegetation conditions, beyond the structural attributes measured in this study may be necessary to fully characterize variations in post-fire effects (Jain & Graham, 2007). Full waveform scanning LIDAR or small footprint discrete return LIDAR instruments would be required to estimate attributes such as canopy bulk density and crown base height (Andersen et al., 2005), which cannot be measured using the discrete return LIDAR profiling system employed in this study.

Another major criticism of remotely sensed measures of burn severity, particularly dNBR, has focused on the influence that pre-fire vegetation has on these measures. The magnitude of dNBR is highly dependent on pre-fire cover, meaning areas with the greatest absolute difference between pre- and post-fire vegetation will have higher burn severity ratings (e.g., areas with relatively more pre-fire vegetation will have higher burn severities than areas with less pre-fire vegetation) (Key & Benson, 2006). Epting and Verbyla (2005) examined the relationship between pre-fire vegetation, burn severity, and post-fire vegetation over a 16-year-period in interior Alaska. They found that pre-fire vegetation did have a strong influence on remotely sensed burn severity: coniferous forest had a higher mean burn severity (using dNBR) than broadleaf forest and shrubland, and mean dNBR increased as tree cover increased and the proportion of area with high severity was greatest in coniferous forest. The impact of pre-fire vegetation on dNBR is particularly problematic in heterogeneous forests (Safford et al., 2008). Hall et al. (2008) likewise concluded that

Fig. 8. (a) Scatterplot with fitting line and 95% confidence interval bands, (b) normal probability plot and raw residuals. Variables: post-fire NBR and absolute change in VF_T.

the magnitude and distribution of dNBR values over boreal forests were influenced by vegetation type. Our results indicate that relationships between post-fire NBR, dNBR, and RdNBR were stronger in dense forests than in open forests and that there was no significant relationship between pre-fire forest structure and post-fire NBR, dNBR, and RdNBR, but there were significant relationships between absolute and relative changes in most of the structural attributes we considered and post-fire NBR, dNBR, and RdNBR. However, in our analysis, we found no marked difference in the relationship between any of the forest structural attributes or forest type and post-fire effects, as characterized by the dNBR and RdNBR.

In response to these criticisms of the NBR and dNBR, Miller and Thode (2007) proposed the RdNBR and posited that the classification of the relative index into severity categories should result in higher accuracies in determining burn severity in heterogeneous landscapes. The ability to more accurately identify high severity areas is important to land managers because high severity areas often have the greatest ecological impacts. Miller and Thode (2007) conclude that the dNBR and RdNBR may be complementary as the dNBR is correlated to the

amount of pre-fire photosynthetically active vegetation, providing an indication of how much vegetation was damaged, while the RdNBR indicates how much vegetation was damaged relative to how much pre-fire vegetation existed. As such, the RdNBR could be useful in areas extensively damaged by insects, such as the current mountain pine beetle epidemic in western Canada, which has resulted in millions of hectares of standing dead pine. It should be noted that while the original NBR was designed to account for both soil and vegetation effects, the dNBR primarily measures changes in vegetation, and as such, may not be useful for directly comparing severity in different areas with different pre-fire vegetation density (Miller & Thode, 2007).

Safford et al. (2008) concluded that RdNBR is better than dNBR where one is interested in quantifying the amount of stand-replacing fire and vegetation mortality on a landscape, because of the dNBR dependence on pre-fire conditions. Hudak et al. (2007) assessed how well remotely sensed burn severity indices related to post-fire effects assessed in the field, by measuring post-fire effects at 418 plots on 50 sites in 8 wildfires across three different ecosystem types. They found
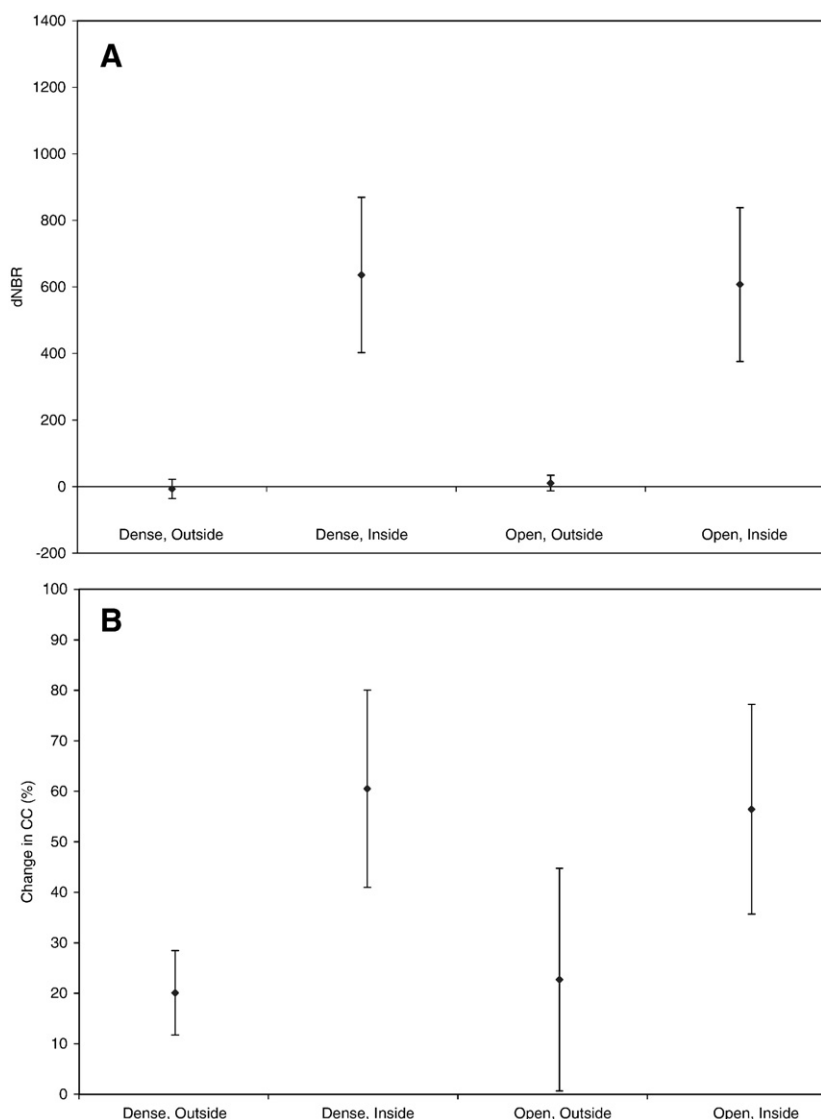
Fig. 9. Mean and standard deviation of (a) dNBR and (b) change in crown closure for dense and open forests, inside and outside the fire perimeter.

that post-fire NBR correlated best with measures of post-fire effects, and concluded that the current practice of using post-fire NBR and dNBR to assess burn severity in the United States was appropriate tools. Hudak et al. (2007) also concluded that the RdNBR may have more limited utility for broad spatial application, since this index only produced better correlations to field data in 1 of the 8 fires they studied, which was an area with similar vegetation cover and density to that in which Miller and Thode (2007) originally developed and applied the RdNBR. Our results support key aspects of Hudak et al. (2007), with one of the strongest relationships we identified as that between absolute change in VF_T and post-fire NBR in dense forests (Table 5).

Our results suggest that the utility of the forest structural measures we have presented may depend on the type of vegetation present and the characteristics of the fire. For example, trees, although damaged or partially consumed, are rarely completely destroyed by fire. However, even partial consumption of tree crowns can have a large impact on LIDAR measures, explaining the marked average per segment differences in attributes such as AID and CC. The results presented in Table 5 and Fig. 9 also indicate that the dense coniferous forests in our study area may have a more uniform structure, and as a result, changes in forest structural attributes in these dense forests may be easier to characterize than in open forests, which have a more complex and variable structure.

8. Conclusions

Profiling LIDAR transects and Landsat imagery are integrated in this study to characterize the post-fire effects of the 2002 House River fire. Post-fire effects are commonly mapped using spectral indices derived from Landsat TM/ETM+ data and the relationship between these indices and actual post-fire effects on the ground is the subject of ongoing research in different ecological regions with varying cover types and conditions. In this study, we characterize post-fire effects using forest vertical structural attributes generated from LIDAR profiling data collected along the same transect pre- and post-fire. Our results indicate that post-fire effects are spatially variable, that there are significant differences in forest structure before and after the fire, and that these differences in structure are more strongly related to post-fire effects in dense forests than open or sparse forests. Measures of vegetation fill, post-fire and absolute change in crown closure, and relative change in average canopy height are useful for characterizing post-fire effects, whereas measures of average inter-tree distance and volume were not strongly correlated to post-fire NBR, dNBR, or RdNBR. No relationship was found between pre-fire vertical forest structure and post-fire effects, and no marked differences were found in the performance of post-fire NBR, dNBR, and RdNBR for characterizing post-fire effects. The information on vertical forest structure provided by LIDAR is useful

for characterizing post-fire effects, but it does not preclude consideration of other attributes such as vegetation type and moisture, topography, long-term weather patterns, that will also influence variations in post-fire effects.

Acknowledgements

References

Allen, J. L., & Sorbel, B. (2008). Assessing the differenced Normalized Burn Ratio's ability to map burn severity in the boreal forest and tundra ecosystems of Alaska's national parks. *International Journal of Wildland Fire*, *17*, 463−475.

Amiro, B. D., Stocks, B. J., Alexander, M. E., Flannigan, M. D., & Wotton, B. M. (2001). Fire, climate change, carbon and fuel management in the Canadian boreal forest. *International Journal of Wildland Fire*, *10*, 405−413.

Andersen, E., McGaughey, R. J., & Reutebuch, S. E. (2005). Estimating forest canopy fuel parameters using LIDAR data. *Remote Sensing of Environment*, *94*, 441−449.

Arroyo, L. A., Pascual, C., & Manzanera, J. A. (2008). Fire models and methods to map fuel types: The role of remote sensing. *Forest Ecology and Management*, *256*, 1239−1252.

Balshi, M. S., McGuire, A. D., Zhuang, Q., Melillo, J., Kicklighter, D. W., Kasischke, E., et al. (2007). The role of historical fire disturbance in the carbon dynamics of the pan-boreal region: A process-based analysis. *Journal of Geophysical Research*, *112*(G02029), 1−18.

Baxter, G. (2003). *Issues arising from observed fire behaviour in aspen cutblocks during the House River Fire in Alberta in May–June, 2002: A Case Study*. Available online: http://fire.feric.ca/36082001/HouseRiverReport.htm (Accessed January 30, 2009).

Bergeron, Y., Flannigan, M., Gauthier, S., Leduc, A., & Lefort, P. (2004). Past, current, and future fire frequency in the Canadian boreal forest: Implications for sustainable forest management. *Ambio*, *33*, 356−360.

Bond-Lamberty, B., Peckham, S. D., Ahl, D. E., & Gower, S. T. (2007). Fire as the dominant driver of central Canadian boreal forest carbon balance. *Nature*, *450*, 89−93.

Chuvieco, E., & Martin, M. P. (1994). A simple method for fire growth mapping using AVHRR channel-3 data. *International Journal of Remote Sensing*, *15*, 3141−3146.

Cocke, A. E., Fulé, P. Z., & Crouse, J. E. (2005). Comparison of burn severity assessments using Differenced Normalized Burn Ratio and ground data. *International Journal of Wildland Fire*, *14*, 189−198.

Dahlberg, A. (2002). Effects of fire on ectomycorrhizal fungi in Fennoscandian boreal forests. *Silva Fennica*, *36*, 69−80.

Dawson, R. D., & Bartolotti, G. R. (2006). Fire in the boreal forest: Proximate effects on reproduction and long-term consequences for territory occupancy of American kestrels. *Ecoscience*, *13*, 75−81.

DeBano, L. F., Neary, D. G., & Ffolliott, P. F. (1998). *Fires effects on ecosystems*. New York, NY: John Wiley and Sons.

De Santis, A., & Chuvieco, E. (2007). Burn severity estimation from remotely sensed data: Performance of simulation versus empirical models. *Remote Sensing of Environment*, *108*, 422−435.

Diaz-Delgado, R., Lloret, F., & Pons, X. (2004). Statistical analysis of fire frequency models for Catalonia (NE Spain, 1975–1998) based on fire scar maps from Landsat MSS data. *International Journal of Wildland Fire*, *13*, 89−99.

Duffy, P. A., Epting, J., Graham, J. M., Rupp, T. S., & McGuire, A. D. (2007). Analysis of Alaskan burn severity patterns using remotely sensed data. *International Journal of Wildland Fire*, *16*, 277−284.

Epting, J., & Verbyla, D. (2005). Landscape-level interactions of prefire vegetation, burn severity, and postfire vegetation over a 16-year period in interior Alaska. *Canadian Journal of Forest Research*, *35*, 1367−1377.

Epting, J., Verbyla, D., & Sorbel, B. (2005). Evaluation of remotely sensed indices for assessing burn severity in interior Alaska using Landsat TM and ETM+. *Remote Sensing of Environment*, *96*, 328−339.

Flannigan, M. D., Amiro, B. D., Logan, K. A., Stocks, B. J., & Wotton, B. M. (2005a). Forest fire and climate change in the 21st century. *Mitigation and Adaptation Strategies for Global Change*, *11*, 847−859.

Flannigan, M. D., Logan, K. A., Amiro, B. D., Skinner, W. R., & Stocks, B. J. (2005b). Future area burned in Canada. *Climatic Change*, *72*, 1−16.

French, N. H. F., Kasischke, E. S., Hall, R. J., Murphy, K. A., Verbyla, D. L., Hoy, E. E., et al. (2008). Using Landsat data to assess fire and burn severity in the North American boreal forest region: An overview and summary of results. *International Journal of Wildland Fire*, *17*, 443−462.

Giglio, L., Csiszar, I. A., & Justice, C. O. (2006). Global distribution and seasonality of active fires as observed with the Terra and Aqua Moderate Resolution Imaging Spectroradiometer (MODIS) sensors. *Journal of Geophysical Research*, *111*, G02016.

Giglio, L., van der Werf, G., Randerson, J. T., Collatz, G. J., & Kasibhatla, P. (2005). Global estimation of burned area using MODIS active fire observations. *Atmospheric Chemistry and Physics*, *6*, 957−974.

Gillett, N. P., & Weaver, A. J. (2004). Detecting the effect of climate change on Canadian forest fires. *Geophysical Research Letters*, *31*, L18211.

Goetz, S. J., Fiske, G. J., & Bunn, A. G. (2006). Using satellite time-series data sets to analyze fire disturbance and forest recovery across Canada. *Remote Sensing of Environment*, *101*, 352−365.

Graham, R. T., McCaffrey, S., & Jain, T. B. (2004). Science basis for changing forest structure to modify wildfire behavior and severity. *General technical report RMRS-GTR-120* Fort Collins, Co: United States Department of Agriculture, Rocky Mountain Research Stations 43p.

Hall, S. A., & Burke, I. C. (2006). Considerations for characterizing fuels as inputs for fire behavior models. *Forest Ecology and Management*, *227*, 102−114.

Hall, R. J., Freeburn, J. T., de Groot, W. J., Pritchard, J. M., Lynham, T. J., & Landry, R. (2008). Remote sensing of burn severity: Experience from western Canada boreal fires. *International Journal of Wildland Fire*, *17*, 476−489.

Han, T., Wulder, M. A., White, J. C., Coops, N. C., Alvarez, M. F., & Butson, C. (2007). An efficient protocol to process Landsat Images for change detection with Tasselled Cap Transformation. *IEEE Geoscience and Remote Sensing Letters*, *4*, 147−151.

Harper, K. A., Bergeron, Y., Drapeau, P., Gauthier, S., & De Grandpré, L. (2005). Structural development following fire in black spruce boreal forest. *Forest Ecology and Management*, *206*, 293−306.

Henry, M. C., & Hope, A. S. (1998). Monitoring post-burn recovery of chaparral vegetation in southern California using multi-temporal satellite data. *International Journal of Remote Sensing*, *19*, 3097−3107.

Hoy, E. E., Franch, N. H. F., Turetsky, M. R., Trigg, S. N., & Kasischke, E. S. (2008). Evaluating the potential of Landsat TM/ETM+ imagery for assessing fire severity in Alaskan black spruce forests. *International Journal of Wildland Fire*, *17*, 500−514.

Hudak, A. T., Morgan, P., Bobbitt, M. J., Smith, A. M. S., Lewis, S. A., Lentile, L. B., et al. (2007). The relationship of multispectral satellite imagery to immediate fire effects. *Fire Ecology*, *3*, 64−90.

Isaev, A. S., Korovin, G. N., Bartalev, S. A., Ershov, D. V., Janetos, A., & Kasischke, E. S. (2002). Using remote sensing to assess Russian forest fire carbon emissions. *Climatic Change*, *55*, 235−249.

Jain, T. B., & Graham, R. T. (2007). The relation between tree burn severity and forest structure in the Rocky Mountains. In R. F. Powers (Ed.), *Restoring fire-adapted ecosystems: Proceedings of the 2005 National Silviculture Workshop. USDA Forest Service Gen. Tech. Rep PSW-GTR-203* (pp. 213−250)., (Tech. Ed.) Albany, CA: Pacific Southwest Research Station, Forest Service, U.S. Department of Agriculture.

Jain, T., Pilliod, D., & Graham, R. (2004). Tongue-tied. *Wildfire*, *4*, 22−26.

Jia, G. J., Burke, I. C., Goetz, A. F. H., Kaufmann, M. R., & Kindel, B. C. (2006). Assessing spatial patterns of forest fuel using AVIRIS data. *Remote Sensing of Environment*, *102*, 318−327.

Johnstone, J. F., & Chapin, F. S., III (2006). Effects of soil burn severity on post-fire tree recruitment in boreal forest. *Ecosystems*, *9*, 14−31.

Johnstone, J. F., & Kasischke, E. S. (2005). Stand-levels effects of soil burn severity on postfire regeneration in a recently burned black spruce forest. *Canadian Journal of Forest Research*, *35*, 2151−2161.

Kasischke, E. S., Christensen, N. L., & Stocks, B. J. (1995). Fire, global warming, and the carbon balance of boreal forests. *Ecological Applications*, *5*, 437−451.

Kasischke, E. S., Turetsky, M. R., Ottmar, R. D., French, N. H. F., Hoy, E. E., & Kane, E. S. (2008). Evaluation of the composite burn index for assessing fire severity in Alaskan black spruce forests. *International Journal of Wildland Fire*, *17*, 515−526.

Key, C. H. (2005). Remote sensing sensitivity to fire severity and fire recovery. *Proceedings of the 5th International Workshop on Remote Sensing and GIS Applications to Forest Fire Management: Fire Effects Assessment* (pp. 29−39). Universidad de Zaragoza. ISBN:84-96214-52-4.

Key, C. H. (2006). Landscape assessment (LA): Sampling and analysis methods. *USDA Forest Service Gen. Tech. Rep. RMRS-GTR-164-CD.*

Key, C. H., & Benson, N. C. (2006). Landscape Assessment (LA). FIREMON: Fire effects monitoring and inventory system. In D. C. Lutes, R. E. Keane, J. F. Carati, C. H. Key, N. C. Benson, & L. J. Gangi (Eds.), *General technical report RMRS-GTR-164-CD* (pp. LA−1-55). Fort Collins, CO: USDA Forest Service, Rocky Mountains Research Station.

Kuenzi, A. M., Fulé, P. Z., & Sieg, C. H. (2008). Effects of fire severity and pre-fire stand treatment on plan community recovery after a large wildfire. *Forest Ecology and Management*, *255*, 855−865.

Lands Directorate (1986). *Terrestrial ecozones of Canada, Ecological Land Classification No. 19, 1986,* 26 p.

Lecomte, N., Simard, N., Fenton, N., & Bergeron, Y. (2006). Fire severity effects on ecosystem biomass dynamics in coniferous boreal forests of eastern Canada. *Ecosystems*, *9*, 1−17.

Lentile, L. B., Holden, Z. A., Smith, A. M. S., Falkowski, M. J., Hudak, A. T., Morgan, P., et al. (2006a). Remote sensing techniques to assess active fire characteristics and post-fire effects. *International Journal of Wildland Fire*, *15*, 319−345.

Lentile, L. B., Morgan, P., Hudak, A. T., Bobbitt, M. J., Lewis, S. A., Smith, A. M. S., et al. (2007). Post-fire burn severity and vegetation response following eight large wildfires across the Western United States. *Fire Ecology Special Issue*, *3*, 91−108.

Lentile, L. B., Smith, F. W., & Shepperd, W. D. (2006b). Influence of topography and forest structure on patterns of mixed severity fire in ponderosa pine forests of the South Dakota Black Hills, USA. *International Journal of Wildland Fire*, *15*, 557−566.

Lezberg, A. L., Battaglia, M. A., Shepperd, W. D., & Schoettle, A. W. (2008). Decades-old silvicultural treatments influence surface wildfire severity and post-fire nitrogen availability in a ponderosa pine forest. *Forest Ecology and Management*, *255*, 49−61.

Lund, H. (1999). A "forest" by any other name…*Environmental Science and Policy*, *2*. (pp. 125−133).

Marshall, I. B., & Schut, P. H. (1999). *A national ecological framework for Canada*. Research Branch Ottawa, Ontario: Environment Canada, Ecosystems Science Directorate, and Agriculture and Agri-Food Canada.

Masek, J. G., Huang, C, Wolfe, R., Cohen, R., Hall, F., Kutler, J., et al. (2008). North American forest disturbance mapped from a decadal Landsat record. *Remote Sensing of Environment*, *112*, 2914−2926.

Miller, J. D., & Thode, A. E. (2007). Quantifying burn severity in a heterogeneous landscape with a relative version of the delta Normalized Burn Ratio (dNBR). *Remote Sensing of Environment*, *109*, 66–80.

Miller, J. D., & Yool, S. R. (2002). Mapping forest post-fire canopy consumption in several overstory types using multi-temporal Landsat TM and ETM data. *Remote Sensing of Environment*, *82*, 481–496.

Mitri, G. H., & Gitas, I. Z. (2008). Mapping the severity of fire using object-based classification of IKONOS imagery. *International Journal of Wildland Fire*, *17*, 431–442.

Monleon, V. J., Azuma, D., & Gedney, D. (2004). Equations for predicting uncompacted crown ratio based on compacted crown ratio and tree attributes. *Western Journal of Applied Forestry*, *19*, 260–267.

Murphy, K. A., Reynolds, J. H., & Koltun, J. M. (2008). Evaluating the ability of the differenced Normalized Burn Ratio (dNBR) to predict ecologically significant burn severity in Alaskan boreal forests. *International Journal of Wildland Fire*, *17*, 490–499.

Mutlu, M., Popescu, S. C., Stripling, C., & Spencer, T. (2008). Mapping surface fuel models using LIDAR and multispectral data fusion for fire behaviour. *Remote Sensing of Environment*, *112*, 274–285.

Natural Resources Canada (2004a). *Canada's national forest inventory land cover classification scheme. Version 4.0.1.* Victoria, British Columbia: Canadian Forest Service, Pacific Forestry Centre 19 p. Available online: https://nfi.nfis.org/documentation/photo_plot/Land_cover_classification_v4.0.1.pdf

Natural Resources Canada (2004b). *Canada's national forest inventory photo plot guidelines. Version 1.1.* Victoria, British Columbia: Canadian Forest Service, Pacific Forestry Centre 43 p. Available online: https://nfi.nfis.org/documentation/photo_plot/Pp_guidelines_v1.1.pdf

Neary, D. G., Ryan, K. C., & DeBano, L. F. (2005). Wildland fire in ecosystems: Effects of fire on soils and water. *General technical report, RMRS-GTR-42-vol.4* Ogden, UT: U.S. Department of Agriculture, Forest Service, Rocky Mountain Research Station 250 p.

Odion, C., & Hanson, C. T. (2006). Fire severity in conifer forests of the Sierra Nevada, California. *Ecosystems*, *9*, 1177–1189.

Odion, C., & Hanson, C. T. (2008). Fire severity in the Sierra Nevada revisited: Conclusions robust to further analysis. *Ecosystems*, *11*, 12–15.

Parisien, M. A., Peters, V. S., Wang, Y. H., Little, J. M., Bosch, E. M., & Stocks, B. J. (2006). Spatial patterns of forest fires in Canada, 1980–1999. *International Journal of Wildland Fire*, *15*, 361–374.

Pastor, E., Zárate, L., Planas, E., & Arnaldos, J. (2003). Mathematical models and calculation systems for the study of wildland fire behaviour. *Progress in Energy and Combustion Science*, *29*, 139–153.

Patterson, M. W., & Yool, S. R. (1998). Mapping fire-induced vegetation mortality using Landsat Thematic Mapper data: A comparison of linear transformation techniques. *Remote Sensing of Environment*, *65*, 132–142.

Pu, R., Li, Z., Gong, P., Csiszar, I., Fraser, R., Hao, W. M., et al. (2007). Development and analysis of a 12-year daily 1-km forest fire dataset across North America from NOAA-AVHRR data. *Remote Sensing of Environment*, *108*, 198–208.

Pyne, S. J., Andrews, P. L., & Laven, R. D. (1996). *Introduction to wildland fire.* New York: John Wiley and Sons Inc.

Riaño, D., Chuvieco, E., Condés, S., Gonzalez-Matesanz, J., & Ustin, S. L. (2004). Generation of crown bulk density for *Pinus sylvestris* L. from LIDAR. *Remote Sensing of Environment*, *92*, 345–352.

Riaño, D., Chuvieco, E., Ustin, S. L., Salas, J., Rodriguez-Perez, J. R., Ribeiro, L. M., et al. (2007). Estimation of shrub height for fuel-type mapping combining airborne LIDAR and simultaneous colour infrared ortho imaging. *International Journal of Wildland Fire*, *16*, 341–348.

Riaño, D., Meier, E., Allgöwer, B., Chuvieco, E., & Ustin, S. L. (2003). Modeling airborne laser scanning data for the spatial generation of critical forest parameters in fire behaviour modeling. *Remote Sensing of Environment*, *86*, 177–186.

Robichaud, P. R. (2000). Fire effects on infiltration rates after prescribed fire in Northern Rocky Mountain forests, USA. *Journal of Hydrology*, *231–232*, 220–229.

Robichaud, P. R., Lewis, S. A., Laes, D. Y. M., Hudak, A. T., Kokaly, R. F., & Zamudio, J. A. (2007). Postfire soil burn severity mapping with hyperspectral image unmixing. *Remote Sensing of Environment*, *108*, 467–480.

Röder, A., Hill, J., Duguy, B., Alloza, J. A., & Vallejo, R. (2008). Using long time series of Landsat data to monitor fire events and post-fire dynamics and identify driving factors. A case study in the Ayora region (eastern Spain). *Remote Sensing of Environment*, *112*, 259–273.

Rogan, J., & Franklin, J. (2001). Mapping wildfire burn severity in southern California forests and shrublands using Enhanced Thematic Mapper imagery. *Geocarto International*, *16*(4), 89–99.

Roy, D. P., Boschetti, L., & Trigg, S. N. (2006). Remote sensing of fire severity: Assessing the performance of the Normalized Burn Ratio. *IEEE Geoscience and Remote Sensing Letters*, *3*(1), 112–116.

Roy, D. P., Jin, Y., Lewis, P. E., & Justice, C. O. (2005). Prototyping a global algorithm for systematic fire-affected area mapping using MODIS time series data. *Remote Sensing of Environment*, *97*, 137–162.

Ryan, K. C. (2002). Dynamic interactions between forest structure and fire behavior in boreal ecosystems. *Silva Fennica*, *36*, 13–39.

Safford, H. D., Miller, J., Schmidt, D., Roath, B., & Parsons, A. (2008). BAER soil burn severity maps do not measure fire effects to vegetation: A comment on Odion and Hanson (2006). *Ecosystems*, *11*, 1–11.

SAS Institute Inc. (2004). *SAS/INSIGHT 9.1 user's guide, volumes 1 and 2.* Cary, NC: SAS Institute Inc.

Shakesby, R. A., & Doerr, S. H. (2006). Wildfire as a hydrological and geomorphological agent. *Earth-Science Reviews*, *74*, 269–307.

Shatford, J. P. A., Hibbs, D. E., & Puettmann, K. J. (2007). Conifer regeneration after forest fire in the Klamath–Siskiyous: How much, how soon? *Journal of Forestry*, *105*, 139–146.

Skowronski, N., Clark, K., Nelson, R., Horn, J., & Patterson, M. (2007). Remotely sensed measurements of forest structure and fuel loads in the Pinelands of New Jersey. *Remote Sensing of Environment*, *108*, 123–129.

Soja, A. J., Tchebakova, N. M., French, N. H. F., Flannigan, M. D., Shugart, H. H., Stocks, B. J., et al. (2007). Climate-induced boreal forest change: Predictions versus current observations. *Global and Planetary Change*, *56*, 274–296.

Stocks, B. J., Fosberg, M. A., Lynham, T. J., Mearns, L., Wotton, B. M., Yang, Q., et al. (1998). Climate change and forest fire potential in Russian and Canadian boreal forests. *Climatic Change*, *38*, 1–13.

Stocks, B. J., Mason, J., Todd, J. B., Bosch, E. M., Wotton, B. M., Amiro, B. D., et al. (2002). Large forest fires in Canada, 1957–1997. *Journal of Geophysical Research*, *107*, 8149.

Stocks, B. J., Mason, J. A., Todd, J. B., Bosch, E. M., Wotton, B. M., Amiro, B. D., et al. (2003). Large forest fires in Canada, 1959–1997. *Journal of Geophysical Research*, *108*, 1–12.

Stow, D., Peterson, A., Rogan, J., & Franklin, J. (2007). Mapping burn severity of Mediterranean type vegetation using satellite multispectral data. *GIScience and Remote Sensing*, *44*, 1–23.

Sweda, T. (1998). Airborne infrared-laser altimetry of forest canopy profile for extensive and accurate assessment of timber resource and environmental function of forests. *Proceedings of International Symposium on Global Concerns for Forest Resource Utilization. Oct. 5–8, 1998, Miyazaki, Japan*.

Turner, M. G., Baker, W. L., Peterson, C. J., & Peet, R. K. (1998). Factors influencing succession: lessons from large infrequent natural disturbances. *Ecosystems*, *1*, 511–523.

Tymstra, C., Flannigan, M. D., Armitage, O. B., & Logan, K. (2007). Impact of climate change on area burned in Alberta's boreal forest. *International Journal of Wildland Fire*, *16*, 153–160.

Tymstra, C., MacGregor, B., & Mayer, B. (2005). The 2002 house river fire. *Fire Management Today*, *65*, 16–18.

van Leeuwen, W. J. D. (2008). Monitoring the effects of forest restoration treatments on post-fire vegetation recovery with MODIS multitemporal data. *Sensors*, *8*, 2017–2042.

van Wagtendonk, J. W., Root, R. R., & Key, C. H. (2004). Comparison of AVIRIS and Landsat ETM+ detection capabilities for burn severity. *Remote Sensing of Environment*, *92*, 397–408.

Varga, T. A., & Asner, G. P. (2008). Hyperspectral and LIDAR remote sensing of fire fuels in Hawaii Volcanoes National Park. *Ecological Applications*, *18*, 613–623.

Verbyla, D. L., Kasischke, E. S., & Hoy, E. E. (2008). Seasonal and topographic effects on estimating fire severity from Landsat TM/ETM+ data. *International Journal of Wildland Fire*, *17*, 527–534.

Viedma, O., Melià, J., Segarra, D., & García-Haro, J. (1997). Modeling rates of ecosystem recovery after fires by using Landsat TM data. *Remote Sensing of Environment*, *61*, 383–398.

Wimberly, M. C., & Reilly, M. J. (2007). Assessment of fire severity and species diversity in the southern Appalachians using Landsat TM and ETM+ imagery. *Remote Sensing of Environment*, *108*, 189–197.

White, J. D., Ryan, K. C., Key, C. C., & Running, S. W. (1996). Remote sensing of forest fire severity and vegetation recovery. *International Journal of Wildland Fire*, *6*, 125–136.

Woodcock, C. E., & Harward, J. (1992). Nested-hierarchical scene models and image segmentation. *International Journal of Remote Sensing*, *13*, 316–318.

Wright, H. A., & Bailey, A. W. (1982). *Fire ecology, United States and Southern Canada.* New York: John Wiley and Sons.

Wulder, M. A., Dechka, J. D., Gillis, M. A., Luther, J. E., Hall, R. J., Beaudoin, A., et al. (2003). Operational mapping of the land cover of the forested area of Canada with Landsat data: EOSD land cover program. *The Forestry Chronicle*, *279*, 1–9.

Wulder, M. A., & Franklin, S. E. (2001). Polygon decomposition with remotely sensed data: Rationale, methods, and applications. *Geomatica*, *55*, 11–21.

Wulder, M. A., Han, T., White, J. C., Sweda, T., & Tsuzuki, H. (2007). Integrating profiling LIDAR with Landsat data for regional boreal forest canopy attribute estimation and change characterization. *Remote Sensing of Environment*, *110*, 123–137.

Wulder, M. A., & Seemann, D. (2003). Forest inventory height update through the integration of LIDAR data with segmented Landsat imagery. *Canadian Journal of Remote Sensing*, *29*, 536–543.

Yoshikawa, K., Bolton, W. R., Romanovsky, V. E., Fukuda, M., & Hinzman, L. D. (2003). Impacts of wildfire on the permafrost in the boreal forests of interior Alaska. *Journal of Geophysical Research*, *108*.

Zasada, J. C., Sharik, T. L., & Nygren, M. (1992). The reproductive process in boreal forest trees. In H. H. Shugart, R. Leemans, & G. B. Bonan (Eds.), *A systems analysis of the global boreal forest* (pp. 85–125). Cambridge: Cambridge University Press.